Eur Biophys J (2010) 39:723–755
DOI 10.1007/s00249-009-0546-6

REVIEW

Crystal structures of all-alpha type membrane proteins

Karen McLuskey · Aleksander W. Roszak · Yanshi Zhu · Neil W. Isaacs

Received: 9 June 2009 / Revised: 19 August 2009 / Accepted: 26 August 2009 / Published online: 14 October 2009

Abstract Integral membrane proteins are involved in a wide range of essential biological functions and the determination of their three-dimensional structures plays a central role in understanding their function. This review focuses on the structures of one class of integral membrane proteins: the functionally diverse all-alpha type membrane proteins. It gives an overview of all the structures determined by X-ray crystallography, describing each system and structure in turn. It shows that the structures of all-alpha type membrane proteins have made valuable contributions to understanding structure–function relationships in membrane proteins. These range from the first insights into the function of exciting individual proteins to an in-depth knowledge of protein function from entire biological systems.

Keywords Crystal structures · All-alpha type membrane proteins · X-ray crystallography

Introduction

The study of membrane proteins is of fundamental importance in structural biology. Around 30% of the genome encodes for this important class of proteins and they are estimated to be the target of more than half of all prescription drugs. Despite their importance, the structures of relatively few membrane proteins are known and the rate at which new structures are being determined is only a small fraction of that for soluble proteins. In 1985, when the first structure of an integral membrane protein, the reaction centre from photosynthetic bacteria, was reported (Deisenhofer et al. 1985), there were only 268 entries in the Protein Data Bank (PDB). Today, the PDB contains nearly 60,000 entries, with around 700 of these being membrane proteins and approximately 80% being all-alpha type membrane proteins. Of the membrane protein structures available only 203 are regarded as unique structures (White 2009).

The slow rate at which the structures of membrane proteins are determined reflects the many challenges that have to be overcome. Although the adoption of suitably modified high-throughput techniques has greatly increased the success rate for the expression of prokaryotic membrane proteins, finding the optimum detergent and conditions for solubilisation and crystallisation remains a challenging and time-consuming task.

Most of the known structures can be described as belonging to two classes: the alpha-helical (all-alpha type) and the beta-barrel (all-beta type) transmembrane proteins (Lomize et al. 2006). This review focuses on the three-dimensional structures of all-alpha type proteins solved by X-ray crystallography. A variety of structures have been determined from prokaryotic, plant, and eukaryotic sources and from a variety of membranous compartments. From the eukaryotes, structures are available from the plasma membrane, the endoplasmic reticulum, and the mitochondrial inner membrane; from plants, structures are available from the thylakoid membrane; in prokaryotes structures are available from the Gram-positive plasma membrane, the Gram-negative inner and outer membranes, and the archaebacterial membrane. This makes the structures from all-alpha type membrane proteins a functionally diverse and exciting group. In this review, we report on the known

K. McLuskey (✉) · A. W. Roszak · Y. Zhu · N. W. Isaacs
Westchem, Department of Chemistry, Glasgow Biomedical Research Centre, University of Glasgow,
120 University Place, Glasgow G12 8TA, UK
e-mail: k.mcluskey@chem.gla.ac.uk

crystal structures of all-alpha type membrane proteins up to the end of 2007. We have assembled these proteins into biologically relevant groups, provided a précis of the main features and function of each structure and given protein databank (PDB) entry codes for the representative structures.

We have also included Table 1, which summarises all of the unique all-alpha type structures determined until July 2009 (the time of submission of this review). The table is organised into functional classes following the text in this review, with additions where required. For each structure the protein name and species; the resolution of structure determination; the year published; and the PDB and PubMed ID codes are listed.

Photosynthetic membrane proteins

Photosynthesis is the process by which plants, algae, and some bacteria capture light energy and convert it into chemical energy. Historically, photosynthetic proteins were the first membrane proteins to be crystallised. Consequently, a relative abundance of structures and functional data is now available.

Photosynthetic apparatus in purple bacteria

In photosynthetic bacteria, antenna complexes (so-called light-harvesting complexes, LH1 and LH2) capture light energy and transfer it to a reaction centre (RC) complex. In the RC, light energy is used to excite an electron, which passes along the cofactor molecules and results in the reduction of quinone to quinol. Quinol diffuses into the membrane and moves to the cytochrome (Cyt) bc_1 complex. Cyt bc_1 reoxidises the quinol, releasing electrons that return the RC to its initial state via the mobile electron carrier Cyt c_2, and pumps protons into periplasmic space. This results in the formation of a transmembrane proton motive force that drives the production of adenosine triphosphate (ATP) by ATP synthase. Structures of LH2, the RC-LH1 core complex, and Cyt bc_1 from photosynthetic bacteria have all been determined (Fig. 1).

Reaction centre

The first breakthrough in membrane protein crystallography came in 1982 with the crystallisation of the reaction centre from the photosynthetic non-sulfur purple bacterium *Blastochloris* [*Blc*., previously classified as *Rhodopseudomonas* (*Rps*.)] *viridis* (Michel 1982); this soon led to determination of the structure to atomic resolution (Deisenhofer et al. 1985, 1995). The RC from *Blc. viridis* is composed of four polypeptides, the subunits L, M, H, and C, which act as a scaffold holding the 14 cofactors in the correct orientation. This structural framework enables the electron-transfer processes to occur after absorption of a photon and results in the reduction of quinone. The crystal structure of this RC is now known to a resolution of 1.96 Å (Li et al. 2006).

Structures of RCs from *Rhodobacter* (*Rb.*) *sphaeroides* (Feher et al. 1989) and from the thermophile *Thermochromatium tepidum* (Nogi et al. 2000) are similar to that of the RC from *Blc. viridis*. Many structures of wild-type and mutant RCs, mainly from *Rb. sphaeroides*, have been subsequently determined to explore and explain the RC functionality (Abresch et al. 1998; Axelrod et al. 2002; Fritzsch et al. 1998; Fyfe et al. 2004, 2000; Lancaster et al. 2000; McAuley et al. 2000; McAuley-Hecht et al. 1998; Ridge et al. 2000; Roszak et al. 2004; Spiedel et al. 2002; Stowell et al. 1997; Xu et al. 2004).

LH2 complex

Purple bacteria typically contain two types of antenna complexes: LH1 is intimately associated with the RC forming the so-called "core" complex whereas LH2 is arranged more peripherally and is present in variable amounts.

The crystal structure of LH2 from *Rps. acidophila* strain 10050 (McDermott et al. 1995; Papiz et al. 2003; Prince et al. 1997) has two small transmembrane (TM) helices (α and β-apoproteins) assembled into two concentric cylinders with ninefold symmetry. Eighteen bacteriochlorophyll *a* (Bchl *a*) molecules are sandwiched between the inner (α) and outer (β) TM helices to form an overlapping ring. A further nine Bchl *a* molecules are positioned between the outer (β) helices with their bacteriochlorin rings sitting perpendicular to the TM helix axis (Fig. 1). Nine carotenoid molecules are found intertwined between the phytol tails of the Bchl *a*, and span the entire complex performing structural, light-harvesting and photoprotective roles. As well as revealing the arrangement of the pigments the structure provided an insight into the efficient energy transfer mechanisms within the complex and from LH2 to the RC.

The structure of LH2 from *Rhodospirillum molischianum* (Koepke et al. 1996) is similar to that from *Rps. acidophila*, but assembles as an octamer and has some differences in the pigment organisation (Cogdell et al. 1997). Structures of LH2 variants grown under "stressed" conditions (low light and/or low temperature) are also available: nonameric LH3 from *Rps. acidophila* strain 7050 (McLuskey et al. 2001) and octameric LH4 from *Rps. palustris* (Hartigan et al. 2002) have been reported at resolutions of 3.0 and 7.5 Å, respectively.

Table 1 Unique all-alpha type membrane protein structures

Name	Species	Res (Å)	PBD ID	Year published	Pubmed ID (primary citation)
Photosynthetic proteins					
RC					
	Blc. viridis	2.3	1PRC	1995 (1985)*	7877166
	Rb. sphaeroides	3.0	1PSS	1989	8161514
	T. tepidum	2.2	1EYS	2000	11095707
LH2					
	Rps. acidophila	2.5	1KZU	1995	9159480
	Rs. molischianum	2.4	1LGH	1996	8736556
	Rps. acidophila (LH3)	3.0	1IJD	1999	11467938
RC-LH1					
	Rps. palustris	4.8	1PYH	2003	14671305
Cyt bc_1					
	Rb. capsulatus	3.5	1ZRT	2004	16034531
	Rb. sphaeroides	3.2	2FYN	2006	16924113
PSII					
	T. vulcanus	3.7	1IZL	2003	12518057
	T. elongatus	3.5	1S5L	2004	14764885
LHCII					
	S. oleracea	2.7	1RWT	2004	15029188
PSI					
	T. elongatus	2.5	1JBO	2004	12615541
	P. sativum	4.4	1QZV	2003	14668855
Cyt b_6f					
	M. laminosus	3.0	1VF5	2003	14526088
	C. reinhardtii	3.1	1Q90	2003	14647374
Respiratory enzymes					
Complex II					
QFR	*E. coli*	3.3	1L0V	1999	11850430
	W. succinogenes	1.8	2BS2	2006	17024183
SQR	*E. coli*	2.6	1NEK	2003	12560550
	Porcine	2.4	1ZOY	2005	15989954
	Chicken	1.8	2H88	2006	16935256
	A. aeolicus	2.0	3HWY	2009	19487671
Complex III					
Partial	Bovine	2.9	1QCR	1997	9204897
Complete	Bovine	3.0	1BE3	1998	9651245
	Chicken	3.2	1BCC	1998	9565029
	S. cerevisiae	2.3	1EZV	2000	10873857
Complex IV					
	P. denitrificans	2.8	1AR1	1995	9380672
	Bovine	2.8	1OCC	1996	8638158
	Rb. sphaeroides	2.0	2GSM	2006	17050688
Cyt bo_3	*E. coli*	3.5	1FFT	2000	11017202
ba_3-Cyt	*T. thermophilus*	2.4	1EHK	2000	10775261
Complex V					
	S. cerevisiae	3.9	1QO1	1999	10576729
DsbA-DsbB					
	E. coli	3.7	2HI7	2006	17110337

Table 1 continued

Name	Species	Res (Å)	PBD ID	Year published	Pubmed ID (primary citation)
FdhN					
	E. coli	1.6	1KQF	2002	11884747
NarGH1					
	E. coli	1.9	1Q16	2003	12910261
PsrABC					
	T. thermophilus	2.4	2VPZ	2008	18536726
Methane Oxidation					
pMMO					
	M. capsulatus	2.8	1YEW	2005	15674245
Sulfatases					
ES					
	Human	2.6	1P49	2003	12657638
ATPases					
F-type					
	S. cerevisiae	3.9	1QO1	1999	10576729
	I. tartaricus	2.4	1YCE	2005	15860619
	S. oleracea	3.8	2W5J	2009	19423706
V-type					
	E. hirae	2.1	2BL2	2005	15802565
P-type					
Ca^{2+} E1	Rabbit	2.6	1SU4	2000	10864310
Ca^{2+} E2	Rabbit	3.1	1IWO	2002	12167852
Na^{+}/K^{+}	Porcine	3.5	3B8E	2007	18075585
Na^{+}/K^{+}	Shark	2.4	2ZXE	2009	19458722
H^{+}	*A. thaliana*	3.6	3B8C	2007	18075595
Retinal-binding proteins					
Ion-pumps					
BR	*H. salinarium*	2.5	1AP9	1997	9287223
aR-1	*H.* sp aus-1	3.4	1AUZ	2006	9560229
aR-2	*H.* sp aus-2	2.5	1VGO	2006	16540121
HR	*H. salinarium*	1.8	1E12	2000	10827943
SR (II)					
+transducer	*N. pharaonis*	2.1	1H2S	2002	12368857
	N. pharaonis	2.4	1JGJ	2001	11452084
	Anabaena	2.0	1XIO	2004	15459396
XR	*S. ruber*	1.9	3DDL	2008	18922772
G protein-coupled receptors					
Rhodopsin					
	Bovine	2.8	1F88	2000	10926528
	T. pacificus	2.5	2Z73	2008	18480818
β_2-AR					
	Human	3.4	2R4R	2007	17952055
	Human	2.4	2RH1	2007	17962520
β_1-AR					
	Turkey	2.7	2VT4	2008	18594507
A_{2A}					
	Human	2.6	3EML	2008	18832607

Table 1 continued

Name	Species	Res (Å)	PBD ID	Year published	Pubmed ID (primary citation)
Outer membrane proteins					
Wza					
	E. coli	2.3	2J58	2006	17086202
PorB					
	C. glutamicum	1.8	2VQG	2008	18462756
ClyA					
	E. coli	2.3	2J58	2009	19421192
Potassium channels					
KcsA					
	S. lividans	3.2	1BL8	1998	9525859
Fab complexed	*S. lividans*	2.0	1K4C	2001	11689936
Ligand-gated					
MthK	*M. thermoautotrophicum*	3.3	1LNQ	2002	12037559
MlotiK1	*M. loti*	3.1	3BEH	2008	18216238
Kv channels					
KvAP	*A. pernix*	3.2	1ORQ	2003	12721618
Kv1.2	Rat	2.9	2A79	2005	16002581
Kv1.2/Kv2.1	Rat	2.4	2R9R	2007	18004376
Kir channels					
Kirbac1.1	*B. pseudomallei*	3.7	1P7B	2003	12738871
Kirbac1.3/3.1	*B. xenovornans*/Mouse	2.2	1XL4	2007	17703190
NaK					
	B. cereus	2.4	2AHY	2006	16467789
Mechanosensitive channels					
MscL					
	M. tuberculosis	3.5	2OAR	1998	9856938
MscS					
	E. coli	3.7	2OAU	2002	12446901
Open form	*E.coli*	3.5	2VV5	2008	18755969
Acid-sensing channels					
ASIC1					
	Chicken	1.9	2QTS	2007	17882215
Magnesium channels					
CorA					
	T. maritima	2.9	2IUB	2006	16857941
	T. maritima	3.9	2BBH	2006	16598263
MgtE					
	T. thermophilus	3.5	2YVX	2007	17700703
Proton channels					
M2					
	H. influenzae	2.0	3BKD	2008	18235504
Ligand-gated ion channels					
pLGIC					
	E. chrysanthemi	3.3	2VL0	2008	18322461
GLIC					
	G. violaceus	3.1	3EHZ	2009	18987630
$P2X_4$					
	D. rerio	2.9	3EAM	2009	18987633

Table 1 continued

Name	Species	Res (Å)	PBD ID	Year published	Pubmed ID (primary citation)
	D. rerio	3.1	3H9V	2009	19641588
Gas channels					
AmtB					
	E. coli	1.4	1U7G	2004	15361618
Amt-1					
	A. fulgidus	1.5	2B2F	2005	16214888
Rh proteins					
	N. europaea	1.3	3B9W	2007	18032606
	N. europaea	1.9	3B9Y	2007	18040042
Water channels (aquaporins)					
AQP1					
	Bovine	2.2	1J4N	2001	11780053
AQP0					
	Bovine	2.2	1YMG	2004	15377788
AqpZ					
	E. coli	2.5	1RC2	2003	14691544
AQP4					
	Human	1.8	3GD8	2009	19383790
AQP5					
	Human	2.0	3D9S	2008	18768791
GlpF					
	E. coli	2.2	1FX8	2000	11039922
SoPIP2;1					
	S. oleracea	2.1	1Z98	2006	16340961
PfAQP					
	P. falciparum	2.1	3C02	2008	18500352
Aqy1					
	P. pastoris	1.2	2W2E	2009	19529756
Protein conducting channels					
SecYE*β*					
	M. jannaschii	3.5	1RHZ	2004	14661030
SecYEG					
	T. martima	4.5	3DIN	2008	18923516
Fab complexed	*T. martima*	3.2	2ZJS	2008	18923527
Gap junctions					
Cx26					
	Human	3.5	2ZW3	2009	19340074
Intramembrane proteases					
GlpG					
	E. coli	2.1	2IC8	2006	17051161
	H. influenzae	2.2	2NR9	2007	17210913
S2P					
	M. jannaschii	3.3	3B4R	2007	18063795
SppA					
	E. coli	2.6	3BF0	2008	18164727
MAPEG family					
FLAP					
	Human	4.0	2Q7M	2007	17600184

Table 1 continued

Name	Species	Res (Å)	PBD ID	Year published	Pubmed ID (primary citation)
LTC_4S					
	Human	2.2	2UUH	2007	17632546
	Human	3.3	2PNO	2007	17632548
ABC transporters					
BtuCD					
	E.coli	3.2	1L7V	2002	12004122
BtuCD-F					
	E. coli	2.6	2QI9	2007	17673622
Sav1866					
	S. aureus	3.0	2HYD	2006	16943773
HI1470/1					
	H. influenzae	2.4	2NQ2	2007	17158291
$ModB_2C_2A$					
	A. fulgidus	3.1	2ONK	2007	17322901
MsbA					
	E. coli	3.7	3B60	2007	18024585
	V. cholerae	5.3	3B5W	2007	18024585
	S. typhimurium	5.5	3B5X	2007	18024585
$MalFGK_2$-MBP					
	E.coli	2.8	2R6G	2007	18033289
ModBC					
	M. acetivorans	3.0	3D31	2008	18511655
MetNI					
	E. coli	3.7	3DHW	2008	18621668
P-gp					
	Mouse	3.8	3G5U	2009	19325113
MFS transporters					
LacY					
	E. coli	3.6	1PV7	2003	12893935
GlpT					
	E. coli	3.3	1PW4	2004	12893936
EmrD					
	E. coli	3.5	2GFP	2006	16675700
RND and SMR transporters					
AcrB					
	E. coli	3.5	1IWG	2002	12374972
EmrE					
	E. coli	1.9	3B9Y	2007	18040042
MexB					
	P. aeruginosa	3.0	2V50	2009	19361527
H^+/Cl^- antiporters					
ClC					
	S. typhimurium	3.0	1KPL	2002	11796999
	E. coli	3.5	1KPK	2002	11796999
Na^+/H^+ antiporters					
NhaA					
	E. coli	3.5	1ZCD	2005	15988517

Table 1 continued

Name	Species	Res (Å)	PBD ID	Year published	Pubmed ID (primary citation)
MCF transporters					
AAC					
	Bovine	2.2	1OKC	2003	14603310
Neurotransmitter transporters					
GltPh					
	P. horikoshii	3.5	1XFH	2004	15483603
LeuT					
	A. aeolicus	1.7	2A65	2005	16041361
CDF transporters					
Yiip					
	E. coli	3.8	2QFI	2007	17717154
Ion coupled symporters (SSS and NCS1 families)					
vSGLT					
	V. parahaemolyticus	2.7	3DH4	2008	18599740
Mhp1					
	A. aeolicus	2.8	2JLN	2008	18927357
Amino acid transporters					
BetP					
	C. glutamicum	3.4	2W8A	2009	19262666
AdlC					
Fab-complexed	*E. coli*	3.2	3HQK	2009	19578361
AdlC					
	E. coli	3.6	3H5M	2009	19478139
ApcT					
	M. jannaschii	2.4	3GIA	2009	19608859
SNARE family					
SNAP-25					
	Rat	3.4	3HD7	2009	19571812

This table lists the structures of unique all-alpha type membrane proteins available in the PDB up the end of July 2009. Proteins of the same type from different species are classed as unique. Only the original structure of each protein is included, unless two structures were published simultaneously

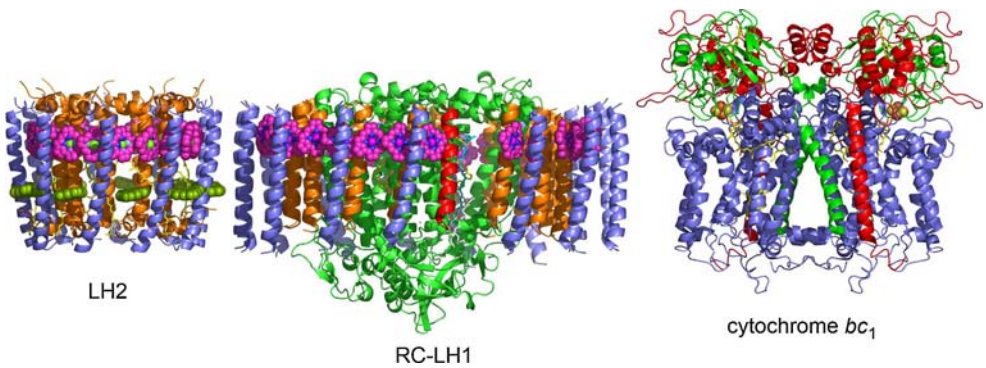

Fig. 1 Photosynthetic apparatus in purple bacteria: LH2, RC–LH1 and cytochrome bc_1. In LH2 and RC–LH1 the α-apoproteins are shown in *orange* and the β-apoproteins in *blue*. Bchl *a* molecules are represented in *olive* (LH2) and *pink* (LH1 and LH2), with their phytyl tails removed for clarity. In RC-LH1 the RC is shown in *green* and the single helix of protein W in *red*. In cytochrome bc_1, the haem pigments are shown in stick representation (with *yellow* bonds) and the 2Fe-2S clusters are shown as *orange* (Fe) and *yellow* (S) van der Waals spheres. All figures were prepared using PyMOL (DeLano 2002)

RC-LH1 "core" complex

The low-resolution (4.8 Å) structure of the RC-LH1 "core" complex from *Rps. palustris* (Roszak et al. 2003), shows the RC closely surrounded by an almost complete oval LH1 complex of 15 pairs of α and β-apoproteins and their coordinated bacteriochlorophylls. An additional single TM helical protein (denoted protein W) is positioned within the inner ring but lacks a partner β-apoprotein in the outer ring, suggesting that it forms part of a gate through which the reduced quinone can move from the RC into the membrane lipid phase (Fig. 1).

Cytochrome bc_1 complex

Low-resolution structures of the Cyt bc_1 complex from *Rb. capsulatus* and *Rb. sphaeroides* have been determined (Berry et al. 2004; Esser et al. 2006) (Fig. 1). Additionally, high-resolution structures of this enzyme from the mitochondrial respiratory electron-transfer chain are also available and, consequently, these are described in detail in the section on respiration.

Photosynthetic apparatus in plants, green algae, and cyanobacteria

In plants, green algae, and cyanobacteria oxygenic photosynthesis converts solar energy into chemical energy by means of three multisubunit membrane protein complexes: photosystems I (PSI) and II (PSII), and cytochrome b_6f (Cyt b_6f). Photosystems capture light from the sun using large antenna complexes (light-harvesting complexes, LHC) and transfer the absorbed energy to their centre, where charge separation analogous to that of the bacterial RC takes place. PSI and PSII form super-complexes with light-harvesting proteins LHCI and LHCII, respectively. Cyt b_6f functionally links PSII and PSI in an electron-transfer process which, coupled with pumping of protons across the photosynthetic membrane, produces a proton gradient that drives ATP synthase. Structural models are available for all of the proteins in this process.

Photosystem II

In plants, the photoinduced oxidation of water is catalysed by PSII, which then facilitates transfer of the resulting electrons to a plastoquinone molecule via a chain of electron carriers. To date, PSII from plants has eluded structure determination. However, structures of PSII core complexes (without light-harvesting Phycobilisomes) from two different species of the thermophilic cyanobacterium *Thermosynechococcus* (T.) have been determined—*T. vulcanus* (Kamiya and Shen 2003) and *T. elongatus* (Biesiadka et al. 2004; Ferreira et al. 2004). These large complexes are composed of 20 subunits, 36 TM helices, and at least 99 cofactors. Overall, the three models are almost identical with regard to the location and orientation of their TM helices and the arrangement of these cofactors.

LHCII

Plant PSII is surrounded by tightly bound trimeric light-harvesting complexes (LHCII) (Barber 2002). These are the major LH complexes of plant PSII and bind half of the chlorophyll molecules found in the thylakoid membrane. The structure of LHCII from spinach (*Spinacia oleracea*) provided a detailed picture of the complex (Liu et al. 2004). The distribution of the pigments found within the trimeric assembly of the monomeric complex favours the efficient absorption of incident light energy from all directions in a broad spectral region. Additionally, this pigment scaffold supports the transfer of the excitation energy to the nearest exit, the putative terminal fluorescence emitter chlorophyll (Chl *a*), in a few steps and at high rates.

Photosystem I

Photosystem I is a highly efficient nano-photoelectric machine that catalyses light-driven electron transfer from plastocyanin (or cytochrome c_6) to ferredoxin, at the stromal side of the membrane.

Elucidation of the structure of PSI from the cyanobacterium *T. elongatus* (Jordan et al. 2001) furnished a detailed picture of 12 protein subunits with 127 cofactors and provided a basis for understanding the high efficiency of the complex in light-capture and electron-transfer. The first structure of PSI from a plant (pea) was determined to 4.4 Å (Ben-Shem et al. 2003) and later to 3.4 Å resolution (Amunts et al. 2007). These structures revealed PS1–LHC1 complexes with 12 core subunits and four peripheral LHC1 proteins. The overall structure is similar to cyanobacterial PSI but with the four LHCI domains assembled in a half-moon shape on one side of the core. The efficient binding of plastocyanin and faster electron transfer in plants can be explained on the basis of these structures.

Cytochrome b_6f

Cyt b_6f mediates electron transport between PSII and PSI and converts the redox energy into part of the proton gradient used for ATP formation.

Structures of two Cyt b_6f complexes from the thermophilic cyanobacterium *Mastigocladus* (*M.*) *laminosus* (Kurisu et al. 2003) and from the algae *Clamydomonas*

reinhardtii (Stroebel et al. 2003) were determined around the same time. Low-resolution structures of inhibitor complexes of Cyt b_6f are also available (Yamashita et al. 2007; Yan et al. 2006). These structures completed the description of the structures of the photosynthetic electron-transport chain with *M. laminosus* Cyt b_6f containing a large quinone exchange cavity where plastoquinone and a novel haem are bound. Additionally, Cyt b_6f has architecture common to the respiratory Cyt bc_1 complexes but the domain arrangement outside the core and the complement of prosthetic groups are markedly different (Smith et al. 2004). This reveals changes in the electron transfer mechanism of the enzyme in response to photosynthesis.

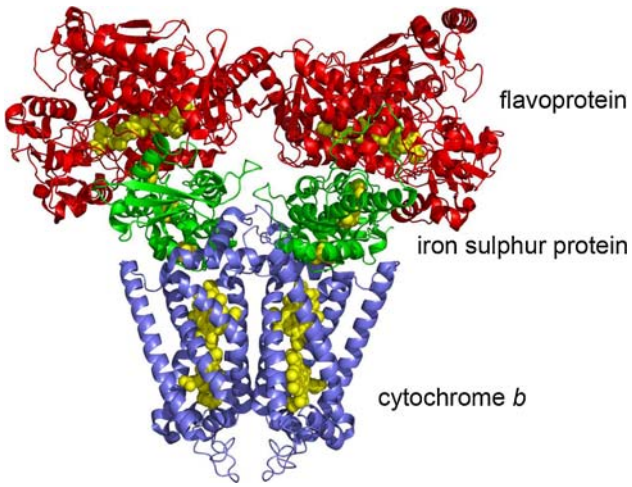

Fig. 2 Structure of fumarate reductase (*QFR*) from *W. succinogenes*. The flavoprotein (*red*), iron-sulfur protein (*green*), and cytochrome *b* (*blue*) subunits form a scaffold for the various prosthetic groups (*yellow*)

Respiratory enzymes

Oxidative phosphorylation

The electron-transport chain in mitochondria is the site of oxidative phosphorylation in eukaryotes. This is a process whereby fatty acids and amino acids are oxidised to produce energy-rich molecules such as ATP and NADH. Respiration is the inverse of photosynthesis. It involves electron transfer and conservation of energy, and requires five respiratory complexes (I–V). Complex I, a proton-pumping NADH:ubiquinone oxidoreductase, has so far eluded structure determination. However, crystal structures have been determined for the respiratory complexes II, III, IV, and V.

Complex II

Succinate dehydrogenase (complex II; or succinate:ubiquinone oxidoreductase, SQR) couples the oxidation of succinate to fumarate in the mitochondria (or the cytoplasm in bacteria) with the reduction of ubiquinone in the membrane. Fumarate reductase (QFR), found in bacteria, is highly homologous to SQR and catalyses the succinate-fumarate interconversion for anaerobic respiration.

Structures of QFR from *Escherichia coli* and *Wolinella succinogenes* (Iverson et al. 1999; Madej et al. 2006) and SQR structures from *E. coli* (Yankovskaya et al. 2003) and from porcine (Sun et al. 2005) and chicken heart (Huang et al. 2006a) mitochondria are available, with several structures of inhibitor complexes (Huang et al. 2006a, b). The structures of QFR revealed the arrangement of the various functional domains (the hydrophilic flavoprotein and iron-sulfur protein subunits, and the membrane-anchor subunits forming cytochrome *b*) (Fig. 2) and consequently the assembly of the various prosthetic groups. This exposed a possible reaction pathway from the quinol-oxidising site in the membrane to the fumarate-reducing site in the cytoplasm.

The hydrophilic subunits of SQR are very similar to those of QFR, although the transmembrane anchor structures are markedly different. The positions of the quinone and ubiquinone-binding sites and the environments of the prosthetic groups provide insight into the functional differences between the two complexes.

Complex III

Ubiquinol-cytochrome *c* oxidoreductase or cytochrome bc_1 (complex III) oxidises the membrane-soluble electron carrier ubiquinol and reduces the water-soluble carrier cytochrome *c*. The first report of a partial structure of Cyt bc_1 from bovine heart mitochondria (Xia et al. 1997) was soon followed by reports of the complete 11-subunit structure from the same source (Iwata et al. 1998), along with structures from chicken mitochondria (Zhang et al. 1998) and *Saccharomyces cerevisiae* (Hunte et al. 2000). Several structures of substrate and inhibitor complexes of this protein from yeast and bovine heart mitochondria have subsequently been determined (Gao et al. 2003; Lange and Hunte 2002; Palsdottir et al. 2003).

These structures revealed an essential dimer that forms a cavity to allow easy shuttling of ubiquinol/ubiquinone to and from the complex and between the hydroquinone oxidation and quinone reduction sites. In addition, various crystal forms of bovine Cyt bc_1 showed the Rieske protein subunit to exhibit significant conformational changes, suggesting a new electron-transport mechanism of the enzyme (Xia et al. 1997). The available crystal structures of this enzyme provide various snapshots along the reaction pathway.

Complex IV

Cytochrome *c* oxidase, or Complex IV, catalyses the transfer of electrons from cytochrome *c* to molecular oxygen and in the process generates a proton gradient across the membrane.

Structures have been determined for a four-protein subunit cytochrome *c* oxidase complex from the soil bacterium *Paracoccus denitrificans* (Iwata et al. 1995) and the complete 13-subunit complex from bovine heart mitochondria (Tsukihara et al. 1996). The three core catalytic subunits in bacterial and mitochondrial enzymes are structurally very similar. Subunit I, the heart of the proton pump, and subunit II contain all the prosthetic groups, and from these the proton translocation pathway was identified. The function of subunit III is more ambiguous but the structure led to the proposal that it could form the entrance to an oxygen-channel leading to the active site. Redox-coupled structural changes in bovine heart cytochrome *c* oxidase, in the fully oxidised, fully reduced, azide-bound and carbon monoxide-bound states have now been determined (Yoshikawa et al. 1998). In addition, a recent high-resolution structure of the complex from *Rb. sphaeroides* (Qin et al. 2006) compares the wild-type and mutant enzymes showing, for the first time, a rearrangement of the water pathway in this enzyme.

Additionally, although *E. coli* lacks both Cyt bc_1 and cytochrome *c* oxidase it has a protein closely related to the latter: ubiquinol oxidase (cytochrome bo_3). This utilizes ubiquinol, and its structure has been solved with its substrate in the active site (Abramson et al. 2000). The structure of the aberrant ba_3-cytochrome *c* oxidase from *Thermus* (*T.*) *thermophilus* has also been determined (Soulimane et al. 2000) and both of these structures add further atomic details to the structural information available for complex IV.

Complex V

The energy from the proton motive force is used by F_1F_o-ATP synthase (complex V) to synthesise ATP. F_1F_0-ATP synthase is a multicomponent complex which has a large globular catalytic domain (F_1) linked to a membrane-embedded F_0 segment which provides the rotational generator to drive this molecular machine. The F_1 domain is an assembly of five subunits with three forming a central stalk linking the other two F_1 subunits to F_0. In most species F_0 has three subunit proteins (*a*, *b* and *c*) with *c* being the most abundant.

The structure of a subcomplex of F_1F_0-ATP synthase, the F_1–c_{10} complex, from yeast mitochondria (Stock et al. 1999) unexpectedly showed the transmembrane motor to be composed of 10 *c*-subunits. This symmetry mismatch between the F_1 and F_0 components led to the suggestion that this could be important in the mechanism by favouring ATP hydrolysis. The structure also provided the first insight into the arrangement of the *c* ring and showed its interactions with stalk subunits. The close contact observed between the central stalk and the *c* ring supports the idea that they rotate together as an ensemble.

DsbA–DsbB

DsbA is a periplasmic cellular catalyst of protein folding that oxidises pairs of cysteine residues to disulfide bonds. On functioning, DsbA is maintained reoxidised by DsbB, an integral membrane protein. The respiratory electron transfer chain participates in the oxidation of DsbA, by acting primarily on DsbB (Kobayashi et al. 1997).

The structure of the DsbA–DsbB oxidase complex from *E. coli* was determined in a form of a disulfide-tethered complex (Inaba et al. 2006). DsbB contains four TM helices and a short periplasmic helix running parallel to the membrane, and the structure of DsbA is almost identical to previously solved structures (Guddat et al. 1998). The structural interface of these two molecules provides insight into DsbB–DsbA molecular recognition and the reaction mechanism of DsbB-mediated DsbA oxidation.

Nitrate respiration

In *E. coli*, respiration of nitrate is the major respiratory pathway in anaerobic environments. The pathway uses formate as an electron donor and leads to reduction of nitrate to nitrite. The two major energy-yielding enzymes in this pathway are formate dehydrogenase-N (FdhN) and nitrate reductase (Nar). These enzymes are believed to translocate protons across the membrane (as for aerobic respiration) by a redox loop, using the quinone pool.

FdhN and NarGH1

The structures of formate dehydrogenase-N (Fdh-N) (Jormakka et al. 2002) and nitrate reductase A (NarGH1) (Bertero et al. 2003) from *E. coli* have been determined. They show a similar subunit organisation to fumarate reductase but in addition they expose a possible proton pathway and provide insights into proton motive force generation by the redox loop.

Methane oxidation

The conversion of the inert hydrocarbon methane to methanol is a difficult reaction to perform and requires some extremely challenging chemistry. Despite this, methanotrophic bacteria catalyse this reaction in the first step

of their metabolic pathway using two forms of the metalloenzyme methane monooxygenase (MMO): soluble MMO (Merkx et al. 2001) (sMMO) and membrane-bound or particulate MMO (pMMO).

pMMO

pMMO from *Methylococcus capsulatus* is composed of three subunits, pmoB (α), pmoA (β), and pmoC (γ) and elucidation of the structure revealed a $\alpha_3\beta_3\gamma_3$ trimer (Lieberman and Rosenzweig 2005). The soluble region of the enzyme is derived mainly from pmoB (Inaba et al. 2006), which consists of two β-barrel structures separated by two TM helices. pmoA and pmoC consist of seven and five TM helices, respectively. Overall, the structure comprises six β-barrel structures supported by 42 TM helices. A hole is formed in the centre of the trimer and widens as it reaches into the membrane. Two copper centres (dinuclear and mononuclear) are located within the soluble domain, although it is unclear from the structure which metal centre is the catalytic site. However, mechanistic clues were derived from cytochrome *c* oxidase (Tsukihara et al. 1995), which is structurally similar to pmoB and also contains a dinuclear copper centre that shuttles electrons into the active site. The structure provides new insight into the molecular details of biological methane oxidation.

Sulfatases

The sulfatase family of enzymes catalyse the hydrolysis of sulfate ester bonds in a wide variety of substrates. A total of 17 human enzymes have been identified to date (Parenti et al. 1997), including one integral membrane protein: estrone/dehydroepiandrosterone sulfatase (ES), which is associated with the membrane of the endoplasmic reticulum (ER) and is one of the enzymes responsible for producing and maintaining high levels of estrogens in breast cancer cells (Billich et al. 2000).

ES

The structure of ES (purified from the human placenta) has been determined (Hernandez-Guzman et al. 2003). It contains two TM helices that traverse the bilayer and a large soluble domain, giving the molecule a "mushroom-like" shape.

The soluble domain consists of two subdomains with the α/β sandwich fold, and closely resembles two known structures of the soluble forms of human sulfatases: aryl sulfatases A (Lukatela et al. 1998) and B (Bond et al. 1997). The catalytic formylglycine was found covalently linked to a sulfate moiety near the top of the TM domain, in the "gill" of the mushroom. The active site location gives information about the functional significance of the membrane association, a possible role for the lipid bilayer in catalysis, and the structure may represent a prototype for enzymes residing in the ER membrane.

ATPases

In general, ATPases catalyse the decomposition of ATP into adenosine diphosphate (ADP) and a free phosphate ion, with release of energy which is used to drive other chemical reactions. Transmembrane ATPases can also function as transport proteins, importing metabolites and exporting toxins and waste products. There are several types of ATPases differing in function (ATP synthesis and/or hydrolysis) and structure. To date, structures are available for P-type, V-type, and F-type ATPases with both the F and V-type containing rotary motors.

F-type

F-ATPase (F_1F_0-ATPase) is another name for F_1F_0-ATP synthase (complex V, described in detail above) found in mitochondria, chloroplasts, and bacterial (inner) membranes. Along with the structure of the F_1–c_{10} complex from yeast mitochondria (Stock et al. 1999), the structure of the rotor of the F-type Na^+-ATPase from *Ilyobacter tartaricus* has also been solved and was found to have a similar symmetry mismatch to the F_1 *c*-ring, as seen in the F_1–c_{10} complex, but with 11 units in the *c* ring (Meier et al. 2005).

V-type

V-ATPases are found in eukaryotic vacuoles and catalyse ATP hydrolysis to transport solutes and to reduce pH in organelles. The structure of the membrane embedded K-ring rotor from the V-type Na^+-ATPase from *Enterococcus hirae* has tenfold symmetry and a K-ring about twice as wide as the *c*-ring in F_0 (Murata et al. 2005). Like the F-type structures, this structure also has an ATP to H^+ stoichiometry of 1–2 (3–6), suggesting favourable ATP hydrolysis and proton pumping by the molecule.

P-type

Phosphorylated-type (P-type) ATPases are found in bacteria, fungi, and in eukaryotic plasma membranes and organelles. They transport ions across the cell membrane by the direct hydrolysis of ATP.

Several structures of P-type calcium ATPases from rabbit have been determined in both their E1 and E2 states, with various substrates bound (Moncoq et al. 2007; Olesen

et al. 2007; Sørensen et al. 2004; Toyoshima and Mizutani 2004; Toyoshima et al. 2000, 2004). More recently, the structures of a related Na^+/K^+ pump from pig kidney (Morth et al. 2007) and a H^+ pump (Pedersen et al. 2007) from *Arabidopsis thaliana* have also been determined. These structures provide insight into how three different pumps deal with their distinct cargoes of ions. Their structural and functional homology indicates they all share the same basic mechanism of ATP-driven ion translocation that will probably apply to all P-type ATPases (Kuhlbrandt 2004).

Retinal-binding proteins

Bacterial rhodopsins are a family of retinal-binding proteins with homologues found in a variety of microorganisms including halobacteria, proteobacteria, cyanobacteria, fungi, and algae (Spudich et al. 2000). All rhodopsins are driven by a common photochemical reaction to carry out one of two distinct functions: light-driven ion transport or photosensory signalling. They all share a common design of a seven TM helical bundle forming an interior pocket for the binding of retinal.

Ion pumps

In halobacteria, bacteriorhodopsin (BR) and halorhodopsin (HR) are light-driven ion pumps for proton and chloride transport, respectively. The structures of several intermediate states of BR, a light-driven ion pump from *Halobacterium* (*H.*) *salinarium* (Pebay-Peyroula et al. 1997) have revealed the pumping mechanism in the enzyme (Luecke et al. 1999). Proton pumps from *Halorubrum* sp. aus-1 and aus-2, archaerhodopsin-1 and 2, respectively, have similar structures (Enami et al. 2006). In addition to these, the 1.8 Å structure of HR from *H. salinarium* (Kolbe et al. 2000) shows key features supporting the idea that chloride and proton transport occur by an equivalent mechanism in the microbial rhodopsins.

Sensory rhodopsin (II)

Sensory rhodopsins I and II (SRI and SRII) found in halobacteria are phototaxis receptors that control the cell's swimming behaviour in response to changes in light intensity and colour (Hoff et al. 1997). They relay signals by protein–protein interactions to integral membrane transducer proteins, which modulate the cell's motility apparatus. The structure of SRII from *Natronobacterium pharaonis* has been determined with (Gordeliy et al. 2002) and without (Luecke et al. 2001; Royant et al. 2001) its transducer. Additionally, a structure of eubacterial SRII from *Anabaena* (Vogeley et al. 2004) has been determined. These structures give information about dynamic protein–protein interactions within the membrane and provide a starting model for transmembrane signal transfer.

G protein-coupled receptors (GPCRs)

Guanine nucleotide-binding protein (G protein)-coupled receptors (GPCRs) activate G-proteins in response to extracellular stimuli. GPCRs detect a remarkable variety of stimuli ranging from neurotransmitters to odorants, and ligand-binding causes conformational changes in the protein that act as a switch to relay signals to the intracellular G-proteins. GPCRs share a variety of structural features, including a bundle of seven TM helices connected by six loops of different lengths.

Rhodopsin

The first GPCR to be elucidated was that of bovine rhodopsin, the light-trapping receptor found in the retina of the eye. Activated by light, it turns on the signalling pathway that leads to vision, and the structure revealed information on the molecular mechanism of GPCR activation (Palczewski et al. 2000). Bovine rhodopsin is the only GPCR available in large amounts from natural sources and for many years various structures of this protein provided a much-needed template for modelling other GPCRs (Li et al. 2004; Okada et al. 2002, 2004; Palczewski et al. 2000; Salom et al. 2006).

β2-adrenergic receptor

In times of stress the adrenal gland releases adrenalin, which activates the β2-adrenergic receptor (β_2AR) to control diverse effects such as rapid pulse and constriction of the blood vessels. Two structures of recombinant human β_2AR were reported in 2007—one with an antibody fragment complexed to the third intracellular loop (Rasmussen et al. 2007) and the other engineered with T4 lysozyme inserted into the same loop (Cherezov et al. 2007) (Fig. 3). Overall, these structures are similar to that of rhodopsin but they do highlight important differences between the ligand-binding sites and potential pathways from these sites to regions that interact with G proteins.

Outer membrane polysaccharide export proteins

Gram-negative bacteria transport a large variety of macromolecules across their outer membranes. These include high-molecular-weight polysaccharides, which must be exported from the cell without compromising the membrane. Two major pathways are involved in the assembly and export of most polysaccharides: the Wzy-dependent

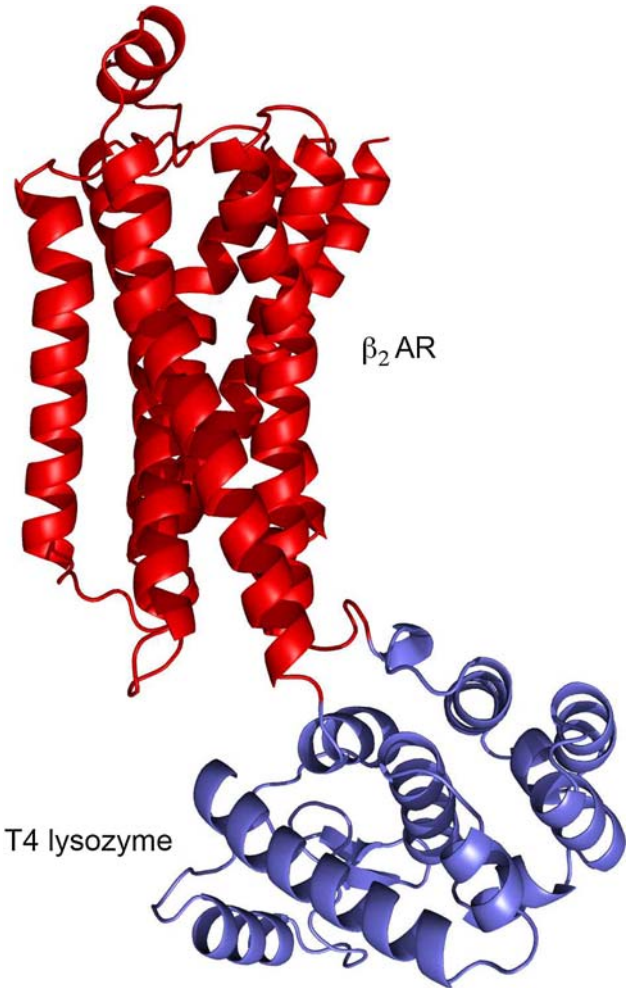

Fig. 3 Structure of a GPCR, the human β2-adrenergic receptor. T4 lysozyme (*blue*) is inserted into the third intracellular loop of the receptor (*red*)

and ATP-binding cassette (ABC) transporter-dependent pathways (for a review see (Cuthbertson et al. 2009)). These involve different components in their inner membrane and periplasmic regions, but both rely on outer membrane polysaccharide export (OPX) proteins for secretion. To date, the only known structure of an integral membrane protein involved in polysaccharide export is the OPX protein Wza from the outer membrane of *E. coli* (Dong et al. 2006).

Wza

Wza forms an octamer with an alpha-helical barrel sitting on top of a large periplasmic structure composed of three domains. Overall the structure is vase-shaped with a large central cavity running along the central axis of the protein. A simple translocation model suggests that the carbohydrate moves from the periplasm to the central cavity of Wza and exits through the helical barrel (Dong et al. 2006). However, Wza is sealed between its central cavity and the periplasm, suggesting that substantial conformational changes occur during the secretion process (Collins and Derrick 2007).

Ion channels

Ion channels are the key elements of electrical signalling in nerve, muscle, and synapse. They respond to diverse signals, for example ligand-binding and changes in transmembrane voltage, opening to allow the passage of ions through their integral membrane section. To achieve this they must form an ion-conduction pathway, be able to select for a particular ion (e.g. K^+ channels) or class of ions (e.g. the cation-selective nicotinic acetylcholine (ACh) receptor channel), and control the opening and closing of the channel; a process known as "gating".

Most ion channels have a similar structural organisation where multiple subunits are arranged around a central pore, with an axis of symmetry running perpendicular to the membrane plane. The pore is the ion conduction pathway and is formed from the interface between the subunits.

Potassium channels

There are two closely related types of potassium (K^+) channels: those containing six TM helices, e.g. the *Drosophila* Shaker K^+ channel family, and those containing only two, e.g. bacterial K^+ channels. Regardless of their size, all functional K^+ channels are composed of four identical subunits, each of which contains a signature sequence critical for discriminating between K^+ and Na^+ ions.

KcsA

The monomeric subunit structure of the K^+ channel from *Streptomyces lividan* (KcsA K^+ channel) (Doyle et al. 1998) consists of two TM helices connected by a short membrane-embedded helix and extended peptide loop. In the active tetrameric structure, these features combine to form the ion-conduction channel, the pore, and the selectivity filter. A later structure of the channel complexed with Fab increased the resolution from 3.2 to 2.0 Å (Zhou et al. 2001), clarified the exact number and configurations of ions in the channel (Fig. 4), and showed that the selectivity filter could exist in two distinct conformations depending on the K^+ ion gradient across the cell membrane.

Ligand-gated channels

Ligand-gated ion channels have ligand-binding domains attached to the pore and use the free energy of ligand

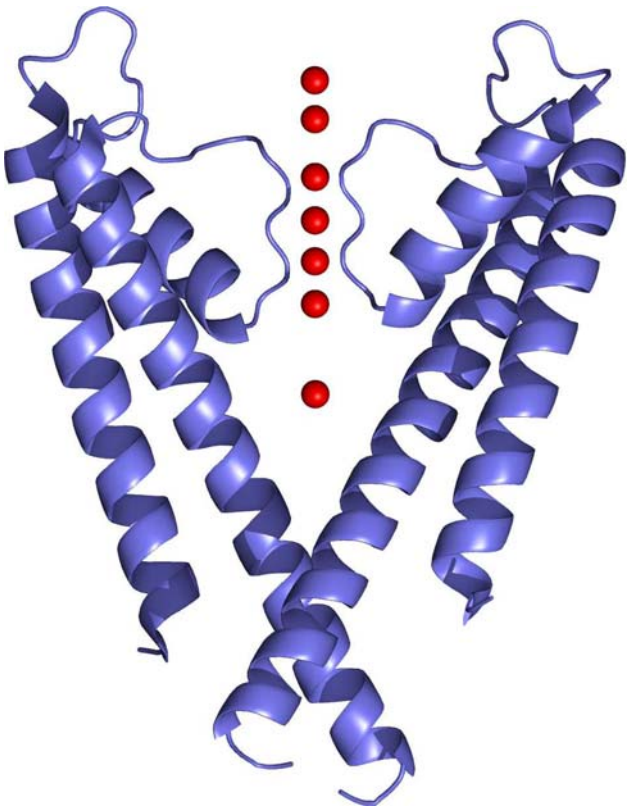

Fig. 4 A cutaway view showing the selectivity filter of KcsA from *Streptomyces lividan.* K^+ ions found along the ion-pathway are shown in *red*

binding to open the channel (Xia et al. 1998). The structure of the ligand (Ca^{2+})-gated K^+ channel from *Methanobacterium thermoautotrophicum* (MthK) (Jiang et al. 2002a) showed the gating machinery (RCK (regulate the conductance of K^+) domains) and a bound ligand (Ca^{2+} ion). The functional channel has a pore similar to that of KcsA and has eight RCK domains, four from the MthK subunits and four that are produced as lone gene products. Comparison of the gating ring from MthK with the *E. coli* RCK domain (Jiang et al. 2001) showed how ligand binding causes the RCK domains to move relative to one another, expanding the diameter of the gating ring and pulling open the pore's inner helices to permit conduction. With Ca^{2+} bound, the MthK structure has an open conformation and a comparison with the closed KcsA structure provides structural insights into gating transitions (Jiang et al. 2002b).

Kv channels

Voltage gated K^+ (Kv) channels are composed of six TM helices (S1–S6) with the first four forming the voltage-sensing domain and S5 and S6, along with an intervening P loop, forming the pore domain (Sigworth 1994). The voltage sensor (VS) is responsible for detecting the change in voltage across the membrane, acting on this change, and converting energy stored in the membrane electric field into mechanical work.

The structures of a full-length Kv channel from *Aeropyrum pernix* (KvAP) and its isolated VS domain were both determined as complexes with monoclonal Fab fragments attached to S3 (Jiang et al. 2002a, 2003). The channel structure is very similar to that of KcsA and only deviates at the glycine-containing gating hinge, where it opens to a distance similar to that found in MthK. Additionally, perimeter helices form an α-helical hairpin—a "paddle" that extends out from the channel into the membrane. This paddle is thought to move between 15 and 20 Å, from one membrane surface to the other, to transport positive charges in response to changes in the membrane potential (Jiang et al. 2004).

The Kv channel complex from rat (Kv1.2, a member of the K^+ *Shaker* channel family) provided an exciting and informative structure of a K^+ channel (Long et al. 2005a). In addition to the integral membrane domains (channel and VS), the structure contained the domain responsible for channel assembly (T1) and a regulatory subunit (β), which sits in the cytoplasm. Expressing the complex with these domains enabled crystallisation without the use of Fab fragments, and provided structures for the pore and VS free of involvement in any crystal contacts. The paddle model proposed for KvAP is also feasible from this structure and a hypothesis of the gating motion from the Kv1.2 structure has been proposed (Long et al. 2005b). It suggests that a downward movement of the S4 paddle, resulting from changes in potential across the membrane, would push down on the S4–S5 linker helices, which in turn compress the inner helices and hence close the pore.

In addition, the structure of a Kv1.2/Kv2.1 chimera (with the VS paddle transferred from Kv2.1 to Kv1.2) from rat (Long et al. 2007), provides an explanation of charge stabilisation within the membrane and additional information for VS movements and pore gating.

Kir channels

Inward rectifying K^+ (Kir) channels act as valves, allowing currents to flow preferentially in the inward direction. Bacterial KirBac1.1 has only two transmembrane segments per subunit (similar to KcsA). The structure of this channel from *Burkholderia* (*B.*) *pseudomallei* was determined as a complete assembly, in the closed state, allowing the main activation gate and structural elements involved in gating to be identified (Kuo et al. 2003). In addition to the conserved pore, Kirbac1.1 has an extra helix, denoted the "slide" helix, that sits perpendicular to the channel at the membrane

interface and is connected, via flexible linkers, to a C-terminal intracellular passageway domain. It can move in response to changes in the C-terminal domain to reposition the inner helices and move a set of four Phe residues that block the conduction pathway.

Two structures of a chimera of KirBac1.3 from *B. xenovorans* with the mouse Kir3.1 have been determined (Nishida et al. 2007). Three quarters of the transmembrane pore of mouse Kir3.1 were replaced with the bacterial pore, leaving the cytoplasmic pore and the membrane interfacial regions of the mouse channel. The structures have different conformations showing possible rigid-body movements in the cytoplasmic pore subunits.

NaK

This non-selective cation channel conducts both Na^+ and K^+ ions and has a structure (Shi et al. 2006) virtually identical with that of KcsA, differing only in the amino-acid sequence of the selectivity filter. In addition, NaK has an interfacial N-terminal helix, which has similarities, in structure and assumed function, to the "slide" helix in KirBac1.1.

Mechanosensitive channels

Mechanosensitive channels allow cells to react to stimuli such as sound, touch, gravity, and pressure (Chang et al. 1998). The two major types of these channels in *E. coli* are MscL and MscS (mechanosensitive channels of large and small conductance, respectively) that act as part of a two-step mechanism to help maintain osmotic balance in prokaryotes.

MscL

To date, the only structure of an MscL channel is that of the closed state, gated channel from *Mycobacterium tuberculosis* (Tb) (TbMscL) (Chang et al. 1998). Like KscA, each subunit contains two TM helices (TM1 and TM2) with the inner helix (TM1) creating the bulk of the pore and the other forming the outside of the channel. TM1 and TM2 are threaded across the membrane in the opposite direction to those found in KcsA. Each TbMscL subunit has an additional cytoplasmic α-helix connected to TM2 by a short loop and these form a five-helix bundle extending the pore of the channel into the cytoplasm. Hydrophobic residues from the inner helices occlude the pore at the cytoplasmic surface and are most likely involved in channel gating (Chang et al. 1998; Ou et al. 1998), modelled as a tilting of the inner helices away from the central axis by sliding over adjacent helices (Sukharev et al. 2001).

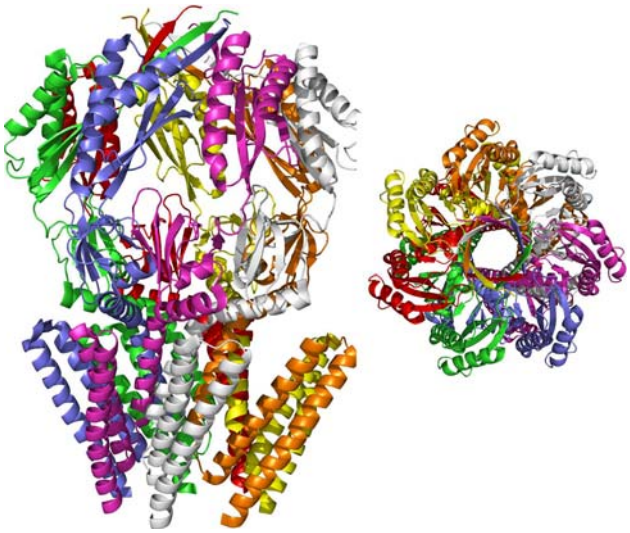

Fig. 5 Structure of the mechanosensitive channel, MscS. Each monomer in the homotetramer is represented by a *different colour*. The diagram on the *right* shows the molecule perpendicular to the membrane plane revealing the open pore

MscS

The structure of MscS from *E. coli* gave insight into a mechanosensitive channel significantly modulated by voltage (Bass et al. 2002). The structure has sevenfold symmetry in the form of a homoheptamer, which consists of a tightly packed TM domain composed of three TM helices (TM1, TM2, and TM3) and two cytoplasmic domains in each subunit (Fig. 5). The middle domain is composed mainly of β-strands and the C-terminal domain is a mixed α/β fold. The three TM helices only partially span the membrane. TM1 and TM2 are connected by a hairpin loop, lie anti-parallel to one another and make very few contacts with other helices in the domain. TM3, along with the loop connecting TM3 to TM2, generates the permeation pathway, in a manner similar to the inner helices in K^+ channels. The overall pore is around 10 Å wide and is assumed to be in an open conformation (Fig. 5). The "voltage-sensor paddle" model proposed for voltage sensing in Kv channels is, in principal, the same general mechanism proposed for voltage-gating in MscS (Bass et al. 2002). The TM1–TM2 helical hairpins are likely candidates for the paddle as they are loosely attached to the periphery of the TM region and contain several positively charged arginine residues.

Acid-sensing ion channels

Acid-sensing ion channels (ASICs) have the highest sodium selectivity of all known ion channels. Found in the neurons of higher vertebrates, they are voltage-independent

and are activated by extracellular protons (H^+) (Waldmann et al. 1997). ASICs belong to a group of proteins known as degenerins that contain two TM regions, two short terminal sections facing the cytoplasm, and a large extracellular domain.

ASIC1

The structure of an ASIC from chicken (Jasti et al. 2007) revealed an unexpected homotrimer, with a large disulfide rich, multi-domain extracellular region. Two helices from each subunit contribute to form a TM domain with an hourglass-shape and an overall negative electrostatic potential in the interior. The conformation of the ion selectivity region is different to that of the K^+ channel; it forms a rather compact mass with no direct passage for ions. However, a number of acidic residue pairs in the "thumb" region of the extracellular domain are proposed to act as proton-binding sites that induce a conformational change leading to gating.

Mg^{2+} channels

Magnesium is unique among the biological cations. Its size, charge density, and hydrated radius are generally different from those of all other cations. In prokaryotes there are three distinct families of Mg^{2+}-transport proteins: CorA, MgtE, and MgtA/B. To date, structures have been determined from both CorA and MgtE family members.

CorA

CorA family members are the primary Mg^{2+} transporters in bacteria and archaea. Two independent structure determinations of a CorA homologue from *Thermotoga maritime* show it to be structurally different from other channels or transporters (Eshaghi et al. 2006; Lunin et al. 2006). CorA is a homopentamer with a large cytosolic domain that funnels into a TM pore composed of two concentric rings of α-helices. It seems to be gated through multiple Mg^{2+} binding sites that serve as Mg^{2+} "sensors".

MgtE

MgtE is widespread in eubacteria and archaea with some species possessing MgtE instead of CorA whereas others possess both channels (Townsend et al. 1995). MgtE from *T. thermophilus* has a different architecture from CorA but a similar gating mechanism (Hattori et al. 2007). MgtE is a homodimer, with the twofold axis normal to the membrane plane. The arrangement of the ten TM helices differs from that of any other channel.

Gas channels

Ammonia transporters

Ammonia gas (NH_3) exists predominantly as the ammonium ion (NH_4^+) when dissolved in water and is the key source of nitrogen for bacteria, fungi, and plants. It is an important nutrient that must be taken up from the surroundings to provide the nitrogen required for amino-acid synthesis, and proteins of the ammonium transport (Amt) family facilitate this process.

Amt proteins are related to the Rh (Rhesus) blood group antigens of mammalian red blood cells. Rh-related proteins are important in critical physiological processes and defects in (or the absence of) these proteins can result in problems with the central nervous system because of ammonium toxicity. The substrate of Rh proteins, NH_3/NH_4^+ (Ripoche et al. 2004; Zidi-Yahiaoui et al. 2005) or CO_2 remains disputed (Peng and Huang 2006; Soupene et al. 2004). Structures of Amt proteins from bacteria (AmtB) and archaebacteria (Amt-1) along with a rare bacterial homologue of a human Rh-protein are available.

AmtB

Functional studies have led to opposing views on whether AmtB transports NH_3 or NH_4^+ through the membrane (Soupene et al. 2002; von Wiren et al. 2000). Two high-resolution structures of *E. coli* AmtB, with and without the presence of ammonia, were published almost simultaneously at resolutions of 1.35 Å (Khademi et al. 2004) and 1.8 Å (Zheng et al. 2004). AmtB is a homotrimer with each individual subunit containing a translocation channel made up of 11 TM helices (TM1–TM11). Similar to other channel structures (e.g. the aquaporins, H^+/Cl^- transporters and SecY) AmtB contains a pseudo twofold axis relating TM1–TM5 to TM6–TM10 (indeterminable from the sequence) with antiparallel architecture.

The hydrophobic nature of the channel itself makes it consistent with the conduction of uncharged NH_3 rather than NH_4^+. The local environment of two His residues in the middle of the channel produce unambiguous hydrogen-bond donors enabling three NH_3 molecules to be stabilized (and observed) within the channel. It has been suggested that Amt/MEP family conducts NH_3 bi-directionally (Soupene et al. 2002) and structurally this appears feasible.

Amt-1

The structure of Amt-1 from the hyperthermophilic archaeon *Archaeoglobus* (*A.*) *fulgidus* is similar to that of *E. coli* AmtB. It exists as a stable trimer, with each monomer consisting of 11 TM helices, and contains a central channel

for substrate conduction (Andrade et al. 2005) (Fig. 6). Xenon was used in the crystal structure to locate hydrophobic cavities in the molecule and confirmed the proposal of NH_3 translocation instead of charged NH_4^+.

Rh proteins

Two structures of Rh proteins from *Nitrosomonas europaea* appeared in the literature at the same time with structure solutions to 1.85 Å (Li et al. 2007) and 1.3 Å (Lupo et al. 2007). The overall structures are very similar to those of the *E. coli* Amt proteins. The structures do not provide definitive support for either NH_3 or CO_2 conduction. However, the absence of a π-cation binding site, proposed to recruit NH_4^+ in Amt proteins, and the identification of a possible conserved CO_2 binding site suggest that the physiological substrate of Rh proteins is more likely to be CO_2 (Li et al. 2007).

Water channels (aquaporins)

Aquaporins (AQPs) are water-specific membrane channels that allow water to move freely and bidirectionally across the membrane (Meinild et al. 1998). The eleven known mammalian aquaporins (AQP0–AQP10; reviewed by King et al. 2004) can be split into two groups: the aquaporins (AQP0–AQP2, AQP4–AQP6 and AQP8), which are generally permeated by water only (although AQP6 and AQP8 are also permeated by anions and urea, respectively; Ma et al. 1997; Yasui et al. 1999); and the aquaglyceroporins (AQPs 3, 7, 9, and 10), which are permeated by water and other small solutes, especially glycerol. *E. coli* contains two AQP homologues: AqpZ, a water permeable channel and GlpF, a glycerol transporter. Crystal structures are available for aquaporins AQP1 (Sui et al. 2001) and AQP0 (Harries et al. 2004), for the plant aquaporin SoPIP2;1 (Tornroth-Horsefield et al. 2006), and for the bacterial homologues AqpZ (Savage et al. 2003) and GlpF (Fu et al. 2000).

AQP1

Elucidation of the structure of AQP1, from bovine red blood cells, revealed a functional tetramer with a pore contained within each monomer (Sui et al. 2001) (Fig. 6). The monomer, consisting of six TM helices and two half-membrane-spanning pore helices, shows pseudo symmetry between its two halves. The dumbbell-shaped pores have two large vestibules at either end of a narrow, constricted, selectivity filter. This filter is unusual in that half of the channel wall can be regarded as hydrophobic and the other half as hydrophilic. This amphipathic pore structure makes sufficient hydrogen-bonding groups available to displace waters of hydration and provide a pathway for coordinating water transport while keeping solute–pore interactions to a minimum. The structure of this channel is not effective for ion transport.

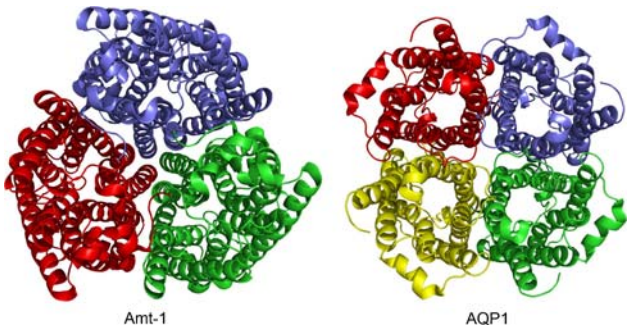

Fig. 6 Structures of a gas (Amt-1) and a water channel (APQ1). The molecules are shown perpendicular to the plane of the membrane, highlighting the pore within the individual monomers. Each monomer is represented by a *different colour*

bAQP0

AQP0 shares 43.6% sequence identity with AQP1 but its water permeability is, approximately, a factor of 40 lower (Chandy et al. 1997). This permeability is reported to double under acidic conditions (Nemeth-Cahalan and Hall 2000) and the pore is reported to close (suggesting some form of gating) at some pHs (Tournaire-Roux et al. 2003). The structure of the protein from bovine lens (bAQP0) has been determined at pH 10.0 (Harries et al. 2004). The overall tetrameric structure is similar to that of AQP1 with the major differences in the pore region. This is much more constricted than in AQP1 with half of the residues substituted with larger more hydrophobic ones. The structure of bAQP0 at high pH (which should, in theory, close the channel) shows eight water molecules in the channel, suggesting an open channel. However, two highly conserved tyrosine residues are involved in the extended constriction of the pore and it is suggested that these limit the flow of water but move out of the channel when required, enlarging the pore size (Harries et al. 2004).

AqpZ

Escherichia coli AqpZ is a highly efficient water channel with the typical aquaporin-fold and channel structure (Savage et al. 2003). Five water molecules were observed in the AqpZ structure and the constriction region is almost identical with that found in AQP1.

GlpF

The *E. coli* glycerol facilitator channel GlpF has the same general folding topology and distribution of pore lining

groups as AQP1 (Fu et al. 2000). The main difference is in the size and nature of its constriction region, where amino-acid substitutions increase its size (1 Å wider) and hydrophobicity. Glycerol molecules located in the filter region have their carbon backbone lined up against the hydrophobic side with the CH–OH groups interacting with the hydrophilic side. This shows the channel achieves both selectivity and conductance by exchanging one set of strict hydrogen bonds for another to closely match successive CH–OH groups. Because polar interactions are only possible on one side of the channel, the hydration shell of an ion cannot be compensated on the hydrophobic side, thereby excluding all ions, even OH^- and H_3O^+.

SoPIP2;1

The structure of the spinach plasma membrane aquaporin SoPIP2;1 was determined in its closed conformation to 2.1 Å resolution and in its open conformation to 3.9 Å resolution (Tornroth-Horsefield et al. 2006). Like other AQPs, SoPIP2;1 crystallised as a tetramer with the most striking difference in the structure being the conformation of an extended loop. In the closed conformation this loop folds underneath the TM domain creating a hydrophobic barrier that blocks the pore from the cytosol. In the open conformation, the structure is more similar to that of AQP1 and the loop is displaced into the cytoplasm. Consequently, this loop provides a flexible lid that caps the channel and then opens after phosphorylation, a gating mechanism that unified a significant body of biochemical and genetic evidence (Johansson et al. 1996, 1998; Tournaire-Roux et al. 2003).

Protein conducting channels

All cellular proteins are synthesised in the cytosol but many then have to be transported through the lipid bilayer to reach their final destination (de Keyzer et al. 2003; Rapoport et al. 1996). This process requires a protein-conducting channel or translocase, which allows newly synthesised proteins to pass through the membrane before folding into their functional tertiary structure (de Keyzer et al. 2003). While ion channels have remarkable specificity in the type of ions they conduct, a translocase has an equally challenging role: it must allow the passage of large and varied substrates (any segment of a translocating protein) to pass through the membrane without compromising the membrane as a barrier to other ions and molecules (Blobel 1980). The structure of SecYEβ in the archaeon *Methanocaldococcus* (*M.*, formerly Methanococcus) *jannaschii* is the only atomic resolution structure of a translocase to date (Van den Berg et al. 2004).

SecYEβ

Translocases are universally conserved heterotrimeric complexes (reviewed by Rapoport et al. 1996) of α, γ, and β subunits with only the α and γ subunits required for channel function. In archaea the three subunits are known as SecY, SecE, and Secβ, respectively, and the complex is denoted SecYEβ.

The structure of SecYEβ from *M. jannaschii* shows that the α subunit contains ten TM helices (whereas both γ and β subunits have only one; Van den Berg et al. 2004) and can be divided into two halves with pseudo-symmetry (as observed in AQPs). The TM helix of the β subunit makes limited contact with the α subunit (suggesting why it is non-essential for function) whereas the TM helix of the γ subunit crosses the membrane at an angle of about 35° acting as a clamp between the two halves of the α subunit. A large cavity forms the pore at the centre of a single SecYEβ complex and funnels down from the cytoplasm into the middle of the membrane where it is blocked by a short distorted helix forming a "plug". This plug would ensure the membrane barrier is not compromised during protein translocation. Displacement of the plug exposes an aqueous channel that narrows in the middle of the membrane as a result of a ring of inflexible, hydrophobic (mainly Ile) residues. These residues are postulated to form a seal around a translocating polypeptide and hinder the passage of small molecules. This structure reveals how the "plug" and the "seal" of SecYEβ could maintain a membrane barrier both co-translocation and post-translocation.

Intramembrane proteases

Intramembrane proteases are a relatively recently discovered class of proteases. They comprise diverse families, which are thought to cleave the TM domain of other membrane-spanning proteins and consequently have their active site embedded within the hydrophobic region of the lipid bilayer. Protein structures are available from two families of intramembrane proteases: the rhomboid family of serine proteases (Lemieux et al. 2007; Wang et al. 2006) and the site-2 protease (S2P) family of metalloproteases (Feng et al. 2007).

Rhomboid family

GlpG

This protein structure, from the rhomboid family of serine proteases, has been determined from both *E. coli* (Ben-Shem et al. 2007; Wang et al. 2006; Wu et al. 2006) and

Haemophilus (*H.*) *influenzae* (Lemieux et al. 2007). The structures from *E. coli* were obtained from independent laboratories and crystallised in different space groups, allowing a rare opportunity to see how crystallisation conditions can affect the functional interpretation of the structure (White 2006). All the structures have six TM helices with the catalytic dyad located near the N-termini of two helices, lying approx. 10 Å below the extracellular surface of the membrane bilayer. A water-filled cavity houses the catalytic residues and a gap located in the cavity is a suggested access route for substrates. The *H. influenzae* structure is very similar to those from *E. coli*, although subtle differences in the active site enabled identification of the oxyanion hole, an essential feature for serine peptidases (Lemieux et al. 2007).

S2P family

S2P

The site-2 protease family require zinc for activity (Brown et al. 2000) and share no apparent sequence homology with the rhomboid proteases. The structure of the TM core of S2P from *M. jannaschii* has six TM helices and a catalytic zinc atom coordinated ~14 Å into the lipid membrane bilayer (Feng et al. 2007). The overall topology is different to that of GplG and the two proteases have no obviously similar features. Despite this, water molecules seem to gain access to the active sites (coordinated zinc and catalytic diad) in a similar manner and they are proposed to have comparable gating mechanisms (Feng et al. 2007).

Membrane-associated proteins in eicosanoid and glutathione metabolism

Despite their name, members of the membrane-associated proteins in eicosanoid and glutathione metabolism (MAPEG) are integral membrane proteins. They are involved in the arachidonic-derived biosynthesis of mediators of pain, fever, and inflammation, and molecules implicated in hypersensitivity conditions such as asthma and allergies (Funk 2001). Most family members depend on glutathione (GSH) for activity, similar to the larger family of cytosolic glutathione transferases (GSTs) (Pearson 2005). Structures are available for human proteins involved in the 5-lipoxygenase pathway (Samuelsson et al. 1987), which converts arachidonic-acid (AA) to cysteinyl leukotrienes (LTC_4 and its metabolites, LTD_4 and LTE_4). These compounds are implicated in hypersensitivity conditions and comprise the slow-reacting substance of anaphylaxis (Samuelsson 1983).

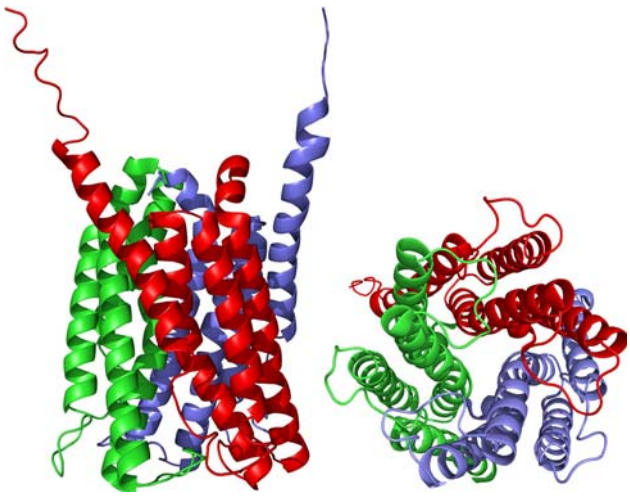

Fig. 7 Structure of human FLAP. Each monomer within the homotrimer is represented in a *different colour* and the molecule is viewed parallel (*LHS*) and perpendicular (*RHS*) to the membrane plane

FLAP

The first elucidation of the structure of an MAPEG family member was that of human 5-lipoxygenase-activating protein (FLAP) in a complex with an inhibitor (Ferguson et al. 2007). FLAP is involved in the first two steps of the conversion of AA to LTA_4 (the unstable precursor to LTC_4), functioning as both a membrane anchor for 5-lipoxygenase (5-LO) and as an AA-binding protein (reviewed by Hebert and Jegerschold 2007). FLAP contains four TM helices and crystallises as a homotrimer with extensive intersubunit contacts (Fig. 7). Three membrane-embedded pockets, found between the monomers, contain the inhibitor binding sites. There is a large cavity at the bottom of the trimer, open to the lumen and extending to around the middle of the membrane. Three distinct entry crevices lead to the entrance of the cavity, which (with the constriction site) is negatively charged while the interior is largely hydrophobic. This structure gives insight into the transfer of AA to 5-LO by FLAP and how FLAP inhibitors prevent this process (Ferguson et al. 2007).

LTC_4S

LTC_4 synthase (LTC_4S) is responsible for the conjugation of LTA_4 with GSH to produce LTC_4, a key step in cysteinyl leukotriene formation. Structures of the apo (Martinez Molina et al. 2007) and GSH-complexed enzymes (Ago et al. 2007; Martinez Molina et al. 2007) have been published.

Like FLAP, LTC_4S is a homotrimer with each monomer containing four TM helices. Additionally, LTC_4S contains a short solvent-exposed helix and long cytoplasmic loop connecting two of the TM helices. The active site,

identified by bound GSH, is buried at the interface between two monomers at the top of a V-shaped cleft that is open towards the cytoplasmic side of the membrane. It is separated from the bulk solvent by the long loop, which would enable conjugation of GSH with LTA_4 to proceed in the required hydrophobic environment. The apo structure is almost identical to the GSH-bound structure with only small adjustments in side-chain positions of this loop (Martinez Molina et al. 2007).

Both complexed structures show that the active site imposes a horseshoe (or U)-shaped conformation on GSH, which is quite distinct from the extended conformation observed in cytosolic GSTs (Holm et al. 2006). They also contain a molecule of *n*-dodecyl-*β*-D-maltoside (DDM), found extending into the cleft, which is suggested to mimic a possible binding mode for LTA_4. These structures enabled proposal of mechanisms for both substrate binding and catalysis.

Transport proteins

Transport proteins overcome the thermodynamically unfavourable process of transporting a substrate against a concentration gradient by coupling to an energetically favourable process. This can be the free energy stored in an electrochemical ion gradient or the movement of a second substrate down the concentration gradient. The cotransported ion/substrate can move in either the same direction or in opposite directions as the substrate and the transporters are termed symporters and antiporters, respectively.

ABC transporters

ATP-binding cassette (ABC) transporters couple the transport of substrates across the cell membrane with the hydrolysis of ATP. They consist of two TM domains (TMDs) that provide a translocation pathway, and two cytoplasmic nucleotide-binding domains (NBDs), that hydrolyse ATP and drive the transport reaction. The NBDs are more highly conserved than the TMDs, which have distinct primary sequences and can vary in the number of TM-spanning helices. ABC transporters import or export a broad range of substrates including amino-acids, ions, sugars, lipids, and drugs into and out of the cell (Holland and Blight 1999). Substrates of ABC exporters enter the translocation pathway from the cytoplasm or from the lipid bilayer, whereas ABC importers require an additional binding protein. To date, six different ABC-transport proteins have had their structures determined.

BtuCD

The vitamin B_{12}-importer from *E. coli*, BtuCD (Locher et al. 2002) is composed of two separate gene products, BtuC, the membrane-spanning subunit, and BtuD, the ATP-binding cassette. The functional unit is a $BtuC_2D_2$ heterotetramer with two copies of BtuD sitting just below the membrane surface in direct contact with two BtuC subunits. A total of 20 TM helices form a single translocation pathway large enough to accommodate vitamin B_{12}. This cavity is closed to the cytoplasm by residues in two loops that appear to function as a gate, giving the channel an outward-facing conformation.

Previous studies on NBDs located the bound nucleotide at the dimer interface between the ABC signature motif of one subunit and the P-loop of the other (Hung et al. 1998). There is, however, substantial separation of the analogous motifs and no nucleotide bound to the BtuD subunits. It has been proposed that the conformational changes generated by the binding and hydrolysis of ATP are transmitted through the interface between the membrane-spanning domains and NBDs and, in particular, through a flexible loop in BtuD (Locher and Borths 2004).

BtuCD-F

BtuF is a periplasmic binding protein that captures vitamin B_{12} and delivers it for uptake, into the cytoplasm, by docking on to BtuCD (Cadieux et al. 2002). Elucidation of the structure of the BtuCD–BtuF (BtuCD–F) complex (Hvorup et al. 2007) revealed its conformation was substantially different from those of BtuCD (Locher et al. 2002) and BtuF (Borths et al. 2002). In this complex BtuF is bound to the periplasmic face of BtuCD. Vitamin B_{12} is absent from the structure and seems to have been lost from the BtuF binding pocket on docking to BtuC. Here, two lobes of BtuF have moved apart allowing two loops from BtuC to insert into the B_{12} binding pocket. The cavity in BtuCD-F is not accessible from either side of the membrane and seems too small to harbour a B_{12} molecule. The TMDs are also asymmetric, and it has been suggested their conformation is intermediate between those of the outward facing BtuCD and the inward facing HI1470/71 (see description below; Pinkett et al. 2007).

Sav1866

One mechanism of drug resistance in bacteria is the active extrusion of drugs from the cell, a process carried out by some transport proteins. Some of these proteins are dedicated to the extrusion of a given drug or class of drugs (for example the tetracycline efflux proteins; Speer et al. 1992) whereas others, the so-called multidrug resistance (MDR) transporters, can handle a wide variety of structurally unrelated compounds (Nikaido 1996; Putman et al. 2000). The structure of Sav1866 from *Staphylococcus aureus* was the first available structure of a bacterial multidrug

transport protein driven by the hydrolysis of ATP (Dawson and Locher 2006).

Sav1866 is a homodimer with each subunit consisting of an amino-terminal TMD (containing six TM helices) and a carboxy-terminal NBD. The two subunits have an unexpected twist, resulting in domain swapping between the TM and NB domains, an arrangement markedly different from that of BtuCD. This transporter was crystallised with a bound nucleotide and showed the transporter in an outward-facing conformation with the central cavity shielded from the cytoplasm and exposed to the extracellular space. The cavity, composed of predominately polar and charged residues, suggests that Sav1866 provides an extrusion pathway with little or no affinity for hydrophobic drugs—rather than a highly specific binding site.

HI1470/1

The HI1470/1 transporter from *H. influenzae* is homologous with BtuCD, belonging to the family of ABC importers that mediate the uptake of metal-chelate species, including haem and vitamin B_{12}. HI1470/1 provided the first structure of an inward-facing conformation for an ABC transport protein and was crystallised without a nucleotide present (Pinkett et al. 2007). The molecular organisation is very similar to that of BtuCD, but unlike BtuCD the permeation pathway is narrow at the periplasmic surface and open to the cytoplasm.

ModB2C2-ModA

The crystal structure of a molybdate ABC importer, $ModB_2C_2$ from *A. fulgidus*, has been determined in a complex with its binding protein, ModA ($ModB_2C_2A$) and in the absence of ATP (Hollenstein et al. 2007). A single ModA molecule, with bound substrate, is attached to the external side of $ModB_2C_2$, with two extracellular loops of ModB contributing to the interface. $ModB_2C_2A$ has 12 TM helices crossing the membrane, in a manner different to that of BtuCD, Sav1866, and HI1470/71, to provide an inward-facing conformation with the cavity only open to the cytoplasm. There is tilting of the NBDs relative to each other, around a hinge at their carboxy termini. This shows that while precise positioning of these domains is required in the ATP-bound molecules there are far fewer geometrical constraints in its absence.

MsbA

MbsA is a member of the MDR ABC transporter family that exports lipid A to the periplasm, and structures showing the molecule in three unique conformations, with and without bound nucleotide, have been determined from three closely related bacterial orthologues: *E. coli* (MsbA-EC), *Vibrio cholerae* (MsbA-VC), and *Salmonella* (*S.*) *typhimurium* (MsbA-ST) (Ward et al. 2007). The structure of MsbA-ST in a complex with 5′-adenylyl-β-γ-imidodiphosphate (AMPPNP) is a dimer with an outward-facing conformation very similar to Sav1866. However, in the absence of nucleotide, MsbA-EC adopts an inward-facing conformation with the NBDs $\sim$50 Å apart and the ATP-binding halves facing each other. MsbA-VC, on the other hand, represents a closed inward-facing conformation with the NBDs much closer to one another. These structures show a large range of motions between the apo-bound and nucleotide-bound states and reveal the movement around a flexible hinge formed by extracellular loops. In MbsA, these observed movements are much larger than those found in the importers BtuCD (Locher et al. 2002) and HI1470/1 (Pinkett et al. 2007). However, MbsA is an exporter that does not interact with a binding protein but is likely to recruit substrates along the periplasmic side of the membrane. MbsA also functions to transport LPS, which contains a large sugar head group and these large conformational changes may be required to accommodate this.

MalFGK2-MBP

The structure of the maltose transporter from *E. coli* was determined in complex with its periplasmic binding partner, maltose binding protein (MBP), its substrate maltose, and ATP (Oldham et al. 2007). The transporter is composed of two integral membrane proteins, MalF and MalG, and two copies of the cytoplasmic ATP-binding cassette MalK ($MalFGK_2$). The structure was determined using a mutant that abolishes ATP hydrolysis and traps ATP in the nucleotide-binding site.

The structure of $MalFGK_2$ is different from that of other ABC transporter structures, because its TMDs are assembled as a heterodimer instead of a homodimer (Fig. 8). However, pseudo twofold symmetry is still observed in the core region of the TM subunits. MalF and MalG are composed of eight and six TM helices, respectively, and the maltose is bound at the interface of these two subunits about halfway into the lipid bilayer. MBP docks on to MalFG at the periplasmic surface in a ligand-free open form making extensive interactions with the TM subunits. These include the insertion of the MalG periplasmic loop into the MBP sugar-binding cleft and several contacts with a large periplasmic loop of MalF [MalF (P2)], which folds into an immunoglobulin-like domain and extends about 30 Å away from the membrane surface.

$MalFGK_2$-MBP shows a similar intertwining of the TMDs as observed in the importer $ModB_2C_2A$ (Hollenstein et al. 2007) and comparison of the two structures reveals striking similarity in the TM regions. These models support

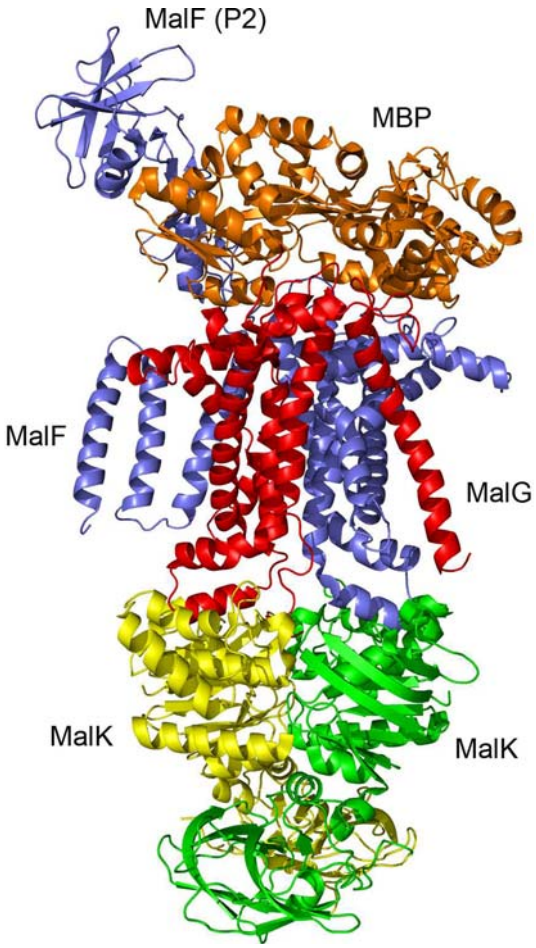

Fig. 8 The ABC-transporter, $MalFGK_2$. MBP (*orange*) docks on to the periplasmic surface of the MalF (*blue*) and MalG (*red*) heterodimer with the MalK (*green and yellow*) ATP-binding domains forming a closed dimer in the cytoplasm

an "alternating access" mechanism in ABC transporters (Jardetzky 1966) with $MalFGK_2$-MBP representing an outward facing catalytic transition state and $ModB_2C_2A$ representing a inward-facing resting state. The MalK subunits form a closed dimer with two ATP molecules bound at the interface, an architecture also observed in the structure of the exporter Sav1866 (Dawson and Locher 2006). These transporters both adopt an outward-facing conformation suggesting that importers and exporters function similarly, by coupling ATP hydrolysis with substrate translocation, except that importers acquire their substrates through interactions with binding proteins (Oldham et al. 2007).

MFS transporters

The major facilitator superfamily (MFS) is the largest family of active transporters, comprising 25% of all transport proteins (Saier 2000). These proteins overcome the thermodynamically unfavourable process of transporting a substrate against a concentration gradient by coupling to an energetically favourable process, such as the free energy stored in an electrochemical ion gradient or the movement of a second substrate down the concentration gradient. Available structures from the MFS currently comprise three *E. coli* transporters: lactose permease, LacY (Abramson et al. 2003b), glycerol-3-phosphate transporter, GltP (Huang et al. 2003) and the multidrug transporter, EmrD (Yin et al. 2006).

LacY

The structure of an inactive mutant of the lactose/H^+ symporter, LacY showed it to be a monomeric protein consisting of 12 TM helices. Like other channel and transport proteins, LacY contains two distinct domains related by pseudo twofold symmetry. The overall structure can be described as "heart shaped" (Abramson et al. 2003a) resulting from a large internal cavity, which is open towards the cytoplasm, suggesting an inward facing conformation. The cavity is largely hydrophilic, accommodates the substrate binding sites, and contains many alanine, proline, and glycine residues, enabling the protein to assume different conformations (Abramson et al. 2004). Residues involved in substrate binding and proton translocation have been extensively studied and it is clear from the structure that the N-terminal domain is responsible for substrate specificity and the protonation site is in the C-terminal domain (Abramson et al. 2003b). Recently the structure of wild-type LacY has appeared in the literature (Guan et al. 2007).

GlpT

GlpT is an inorganic phosphate (P_i)/glycerol-3-phosphate (G3P) antiporter, and although its substrate and translocation process are markedly different from those of LacY, their structures are very similar and superimpose well (Huang et al. 2003). Less is known about substrate specificity in GltP, but binding is known to be mediated by a phosphate moiety. Arg residues found at the closed end of the pore, near the middle of the membrane, are also thought to be involved (Auer et al. 2001) and a mechanism has been proposed (Huang et al. 2003). Both the LacY and GlpT structures support the "alternating access" mechanism of transport (Jardetzky 1966). This suggests that these transporters will undergo a series of conformational changes so that the ligand-binding site is accessible from one side of the membrane or the other, but not from both sides at the same time.

EmrD

EmrD is a multidrug transporter that expels amphipathic compounds across the inner membrane of *E. coli*.

Elucidation of the structure of EmrD (Yin et al. 2006) revealed overall topology similar to those of LacY and GlpT. However, the TM helices that form the internal cavity deviate substantially in their orientation and, consequently, the molecule is less symmetric. Unlike its predecessors, this structure does not adopt a V-shaped conformation and instead seems to form an intermediate state. The most notable difference in this structure is its hydrophobic internal cavity, which is consistent with its role transporting amphipathic molecules. It is thought that two extended periplasmic loops bind substrates directly from the lipid bilayer and, together with the internal cavity, facilitate multi-substrate specificity, binding, and transport.

RND and SMR multidrug transporters

There are many drug-exporter channels in bacteria and these can generally be placed into five separate families, including the ABC and MFS transporters already described. The others are the multidrug and toxic compound extrusion (MATE) (Brown et al. 1999), the resistance nodulation division (RND), and the small multidrug resistance (SMR) families. MATE uses an electrochemical gradient of sodium ions whereas RND and SMR (similar to the MFS transporters) use a proton gradient to drive the extrusion of drugs from the cell. To date, MATE is the only family of multidrug transport proteins that has no representative structure in the PDB.

AcrB

The first structure of a multidrug efflux transporter to be determined was that of the *E. coli* protein AcrB from the RND transport family (Murakami et al. 2002). RND transporters generate resistance by forming part of a tripartite complex, with a membrane fusion protein (MFP) and an outer membrane protein, to pump drugs out of the cell directly into the external medium (Nikaido 1998). AcrB forms a complex with MFP AcrA and outer membrane channel TolC and has the widest substrate specificity among all known multidrug pumps (Nikaido 1996). The structure of AcrB has been determined in the absence (Murakami et al. 2002) and presence (Murakami et al. 2006) of bound substrates, complexed with four structurally dissimilar ligands (Yu et al. 2003) and a single TM subunit (Tornroth-Horsefield et al. 2007), and determined from two different crystal forms showing asymmetry in the trimer (Seeger et al. 2006).

The TM region of AcrB contains 36 TM helices (12 from each subunit) and the protomers pack loosely to form a large (30 Å in diameter) TM hole, open at both cytoplasmic and periplasmic sides, crossing the entire lipid bilayer. The two periplasmic domains make up a large 70 Å long headpiece for AcrB. The pore domain sits directly on the TMD and the TolC docking domain sits on top of the pore domain opening like a funnel to the outside of the cell and leading down into the pore. The structure suggests that substrates may be collected and exported in one of two ways: from the periplasm, through the large vestibules in the pore domain, and from the inner leaflet and the cytoplasm, through a TM groove at the periphery of each TM domain. The structures of the drug–AcrB complexes (Yu et al. 2003) showed three types of ligand molecules bound simultaneously, primarily via hydrophobic interactions, to the large central cavity, with each structurally distinct ligand using a slightly different subset of AcrB residues.

EmrE

Overexpression of the *E. coli* multidrug transporter EmrE causes the bacteria to become resistant to a wide variety of toxic cationic hydrophobic compounds (Yerushalmi et al. 1995). It has over 60 homologues in both Gram-negative and Gram-positive bacteria (Schuldiner et al. 2001) and is a member of the SMR family of transporters. Amongst MDR transporters the SMR family has the simplest organisation and EmrE is the smallest, with only 110 amino-acid residues. It is a hydrophobic protein with only eight charged residues, including a completely conserved glutamine, which is essential for activity (Yerushalmi and Schuldiner 2000).

Low-resolution structures of EmrE with and without bound substrate (tetraphenylphosphonium; TPP) have been determined (Chen et al. 2007). This small, four TM helical protein binds TPP as an antiparallel homodimer. Three of the four helices from each monomer are involved in substrate binding, with the fourth contributing to the dimerisation of the molecule. The unusual antiparallel conformation observed in the crystal structure supports the idea that EmrE monomers are inserted into the *E. coli* membrane in two different orientations (Rapp et al. 2007).

H^+/Cl^- antiporters

H^+/Cl^- (ClC) antiporters (formerly described as chloride channels; Pusch et al. 2006) are found in both prokaryotic and eukaryotic cells. The flow of Cl^- ions in one direction is stoichiometrically coupled to the movement of protons in the opposite direction, controlling salt and water levels across the cell membrane. They select anions over cations and show a strong correlation between ion-conduction and gating, as a certain amount of Cl^- is required to open the pore (Chen and Miller 1996; Pusch et al. 1995).

EcClC and StClC

The structures of two ClC transporters from *S. typhimurium* (StClC) and *E. coli* (EcClC) are structurally similar (Dutzler et al. 2002). They contain two identical subunits, each consisting of 18 TM helices, which show pseudo twofold symmetry. Each subunit creates its own pore and selectivity filter creating two conduction pathways per functionally active dimer.

In both structures, highly conserved regions, found at the N-terminal loops of pseudo symmetry-related helices, come together, resulting in partial positive charges from the helix dipoles pointing towards the ion-binding site where a Cl^- ion is found. Water-filled vestibules from the extracellular and intracellular solutions reach into this site, preventing the ion from binding too tightly. The ends of the helices point into the aqueous solution, which could help direct ions into the active site. A conserved glutamate residue sits just above the bound Cl^- ion, blocking the pore. Structural and mutagenesis studies on an EcClC–Fab complex structure have shown this to be the channel's gate (Dutzler et al. 2003). This led to a proposal of a simple gating mechanism whereby an open gate would transport ions through three ion-binding sites, providing a queue of anions to connect the intracellular and extracellular solutions.

Na^+/H^+ antiporters

The ability of cells to adapt to high salt concentrations or extreme pH values is crucial for their viability. Na^+/H^+ antiporters function in achieving this by exchanging Na^+ for H^+ ions across the cytoplasmic membrane and many other intracellular membranes. In mammals, dysfunction of one such transporter, NHE1, is associated with many pathological conditions including heart disease and cancer (Slepkov et al. 2007). Many of these proteins are tightly regulated by pH (Padan et al. 2004), including NhaA, the main Na^+/H^+ antiporter in *E. coli*, which is currently the only Na^+/H^+ antiporter available as a three-dimensional structure (Hunte et al. 2005).

NhaA

The function of NhaA is down-regulated at acidic pH (Padan et al. 2004), a phenomenon used to obtain the crystal structure of the protein at pH 4.0 (Hunte et al. 2005). NhaA contains 12 TM segments, organised into two densely packed domains of six TM segments. One of the domains shows pseudo-symmetry, as observed in other transporters; the other forms a linear bundle of six TM helices. At the domain interface, a negatively charged funnel runs in opposite directions from the centre of the membrane separated by a barrier of densely packed, non-polar residues. The passage through the funnel narrows towards the membrane and is lined by nonpolar residues, so Na^+ or Li^+ cannot access the binding site in this conformation (Hunte et al. 2005). This inactive conformation is not surprising, given the acidic pH at which the protein was crystallised. The pH sensor of NhaA is found at the mouth of the cytoplasmic funnel, which is separate from the substrate-binding site found in the middle of the membrane. The sensor, a distorted helix, protrudes into the cytoplasm and has the flexibility to enable long-range conformational changes. It has been proposed that at alkaline pH a conformational change in this sensor would result in reorientation in NhaA that would remove the periplasmic barrier and consequently expose the substrate-binding site.

MCF transporter family

Transport through the inner membrane of mitochondria is achieved by a large family of transport proteins termed the mitochondrial carrier family (MCF) (Walker and Runswick 1993). They transport a broad variety of metabolites and cofactors across the mitochondrial inner membrane, making them essential for eukaryotic metabolism. The only structure available from this family is of an ATP/ADP carrier (AAC) protein (Pebay-Peyroula et al. 2003).

AAC

In mitochondria, regeneration of ATP occurs in the mitochondrial matrix, requiring ADP to be imported into the matrix while ATP is exported into the cytoplasm. This import of ADP and export of ATP is carried out by the AAC antiporter. The structure of AAC from bovine heart mitochondria in complex with an inhibitor, carboxyatractyloside (CATR), is monomeric and contains six TM helices (Pebay-Peyroula et al. 2003). These form a compact cone-shaped barrel only accessible from the intermembrane space (IMS) and closed towards the matrix surface, by three amphipathic surface helices sitting parallel to the membrane. CATR, thought to bind in the ADP binding site (Gropp et al. 1999), is found buried deep within the pit and interacts most strongly with residues found near the bottom. These residues block the channel, and it has been suggested they are responsible for AAC's specificity for adenine nucleotides. This open structure is thought to represent a conformation of AAC that is ready to bind ADP from the IMS (Pebay-Peyroula et al. 2003) and that a conformational change from a "pit" to a "channel" would be required for substrate translocation. Elucidation of the structure of a second crystalline form of AAC revealed that the biological dimer is mediated by two cardiolipins sandwiched between the monomers, on the matrix side of the protein (Nury et al. 2005).

Neurotransmitter transporters

In the brain, neurons communicate primarily through neurotransmitters, which must be cleared from the cell soon after release by the neurons. In eukaryotes two major families of proteins are responsible for this process (Gouaux 2009). These differ in both primary sequence and atomic structure and are generally described as the glutamate/neutral amino acid transporter family SLC1 (Kanai and Hediger 2004) and the neurotransmitter sodium symporter (NSS) or SLC6 family (Chen et al. 2004). Crystal structures are available for bacterial homologues from each family.

GltPh

The first neurotransmitter transporter (and the first amino-acid transporter) structure to be obtained was that of the prokaryotic sodium-dependent glutamate transporter from *Pyrococcus horikoshii* (GltPh) (Yernool et al. 2004). Glutamate is the predominant excitatory neurotransmitter in the mammalian central nervous system and glutamate transporters are responsible for reuptake of glutamate, which would otherwise be toxic, from the extracellular surface of nerve cells (Danbolt 2001). In prokaryotes, glutamate uptake is coupled to the cotransport of protons and/or sodium ions (Slotboom et al. 1999).

The overall structure of GltPh is a homotrimer with an unusual "bowl-shaped" conformation (Yernool et al. 2004), with a large hydrophilic basin facing the extracellular space and the base of the bowl sitting towards the cytoplasm. Each subunit provides a wedge of the bowl and contains eight TM helices and two C-terminal helical hairpins. The TM domain has no internal symmetry but the hairpin loops can be superimposed with an rmsd of 2.4 Å, even though they have no significant sequence identity (Yernool et al. 2004).

A putative substrate molecule is found between the hairpin loops (in each monomer) situated ~5 Å from the bottom of the basin in an occluded site, protected from the solution on both sides. There is no pathway large enough in the structure for substrate transport and consequently substrate release would require a conformational change of the protein. It is suggested that the large basin enables substrates to cross the membrane to within 5 Å of the binding site. The hairpin loops then act as gates from the intra and extra-cellular solutions to allow the substrates access from either side of the membrane (Slotboom et al. 1999). In addition, the structure of GltPh with a bound inhibitor revealed a conformation open to the extracellular space, with one of the hairpin loops shifting about 10 Å (Boudker et al. 2007).

LeuT

The NSS family of transporters pump neurotransmitters across the membrane using Na^+ and Cl^- electrochemical gradients as sources of energy. In humans, functional impairment of these transporters contributes to multiple disorders including depression, Parkinson's disease, and epilepsy (Hahn and Blakely 2002; Richerson and Wu 2004). They are also the targets for substances such as cocaine and Prozac (Amara and Sonders 1998; Blakely 2001), which have a profound effect on brain function.

The crystal structures of LeuT, a bacterial leucine NSS transporter from *Aquifex aeolicus* (Yamashita et al. 2005), and of LeuT in complex with tricyclic antidepressants (Singh et al. 2007; Zhou et al. 2007) have been determined. The functional monomer of LeuT contains 12 TM helices, with pseudo twofold symmetry. Leucine is found in the centre of the protein in a dehydrated binding site. It sits close to two Na^+ ions and makes a direct contact, through its carboxy group, to one of these. This shows that the coupling between the driving ion and the substrate is direct and that the sodium ions are likely to be required to organise and stabilize the binding site. Preferential binding of Na^+ over K^+ seems to be the result of the sodium binding sites being too small to accommodate the larger K^+ ion. Because the binding site is devoid of water, it must form precise binding sites to compensate for the energetically unfavourable dehydration of Na^+.

The substrate-binding site is occluded (as observed in GltPh) from both sides of the membrane, although the thickness of the obstructing protein is much smaller towards the extracellular side of the membrane. This suggests that access to the binding site from the outside would require fewer conformational changes than would be required for access from the inside or cytoplasmic solution (Gouaux 2009). It is also proposed that the transport mechanism involves substrate-binding and ion-binding to stabilise different conformations in helices that lead to opening or closing of the gates (Yamashita et al. 2005).

CDF transporters

The cation diffusion facilitator (CDF) family of proteins transport heavy metals including cobalt, cadmium, and zinc, preventing metal build-up in cells (Maser et al. 2001). Unusual sequence divergence and size variation is apparent, and in eukaryotes they are found in both plasma and organellar membranes. These proteins are secondary carriers that utilize the proton motive force and are likely to function as H^+ antiporters (for ion efflux) or H^+ symporters (for ion uptake). Only one structure of a CDF family member is available in the PDB—that of Yiip, a bacterial homologue of a CDF zinc transporter.

Yiip

Yiip catalyses Zn^{2+}/H^{+} exchange across the inner membrane of *E. coli* and its structure has been determined in complex with zinc (Lu and Fu 2007). Yiip is a homodimer with each protomer containing six TM helices and a cytoplasmic domain that adopts a metallochaperone-like fold. The cytoplasmic domains are held together by four Zn^{2+} ions at their interface, whereas the TM domains are clearly separated, swinging out in a Y-shaped conformation. An important tetrahedral Zn^{2+} binding site is located in a water-filled cavity that is open to both the periplasm and the membrane bilayer. This large extracellular cavity penetrates more than half of the membrane thickness and is located close to a second (ion-free) intracellular cavity with no connecting channel. There is no obvious pathway through the structure and the mechanism of transport was not apparent from this unusual structure.

Future perspectives

X-ray crystallography has made significant advances in determining the structures of integral membrane proteins over the past quarter century. It is hard to find a single instance where the determination of a new membrane protein structure has not had a major impact in its field. Despite these successes, the rate of progress is slow. However, while the structures determined represent only very sparse sampling of the many varieties of membrane proteins, those available from the all-alpha type represent proteins from an assortment of membranes and a variety of sources. Although there are many common technical difficulties in working with membrane proteins, it seems that each protein family presents a unique set of problems and when these are overcome the structures of others in the family follow quickly. With many more crystallographers taking on the challenge of membrane proteins, and with improvements in techniques and instrumentation, we can expect ever more exciting and interesting structures in the coming quarter century.

Acknowledgments This work has been supported by the BBSRC. KMcL, AWR, and NWI are members of the Membrane Protein Structure Initiative (MPSI). The authors would like to thank Mads Gabrielsen and Frank Kroner for their critical comments.

References

Abramson J, Riistama S, Larsson G, Jasaitis A, Svensson-Ek M, Laakkonen L, Puustinen A, Iwata S, Wikstrom M (2000) The structure of the ubiquinol oxidase from *Escherichia coli* and its ubiquinone binding site. Nat Struct Biol 7:910–917 (PDB id 1FFT)

Abramson J, Smirnova I, Kasho V, Verner G, Iwata S, Kaback HR (2003a) The lactose permease of *Escherichia coli*: overall structure, the sugar-binding site and the alternating access model for transport. FEBS Lett 555:96–101

Abramson J, Smirnova I, Kasho V, Verner G, Kaback HR, Iwata S (2003b) Structure and mechanism of the lactose permease of *Escherichia coli*. Science 301:610–615 (PDB id 1PV7)

Abramson J, Kaback HR, Iwata S (2004) Structural comparison of lactose permease and the glycerol-3-phosphate antiporter: members of the major facilitator superfamily. Curr Opin Struct Biol 14:413–419

Abresch EC, Paddock ML, Stowell MHB, McPhillips TM, Axelrod HL, Soltis SM, Rees DC, Okamura MY, Feher G (1998) Identification of proton transfer pathways in the X-ray crystal structure of the bacterial reaction center from *Rhodobacter sphaeroides*. Photosynth Res 55:119–125

Ago H, Kanaoka Y, Irikura D, Lam BK, Shimamura T, Austen KF, Miyano M (2007) Crystal structure of a human membrane protein involved in cysteinyl leukotriene biosynthesis. Nature 448:609–612 (PDB id 2PNO)

Amara SG, Sonders MS (1998) Neurotransmitter transporters as molecular targets for addictive drugs. Drug Alcohol Depend 51:87–96

Amunts A, Drory O, Nelson N (2007) The structure of a plant photosystem I supercomplex at 3.4 Å resolution. Nature 447:58–63 (PDB id 2O01)

Andrade SL, Dickmanns A, Ficner R, Einsle O (2005) Crystal structure of the archaeal ammonium transporter Amt-1 from *Archaeoglobus fulgidus*. Proc Natl Acad Sci USA 102:14994–14999 (PDB id 2B2F)

Auer M, Kim MJ, Lemieux MJ, Villa A, Song J, Li XD, Wang DN (2001) High-yield expression and functional analysis of *Escherichia coli* glycerol-3-phosphate transporter. Biochemistry 40:6628–6635

Axelrod HL, Abresch EC, Okamura MY, Yeh AP, Rees DC, Feher G (2002) X-ray structure determination of the cytochrome c_2: reaction center electron transfer complex from *Rhodobacter sphaeroides*. J Mol Biol 319:501–515 (PDB id 1L9B, 1L9 J)

Barber J (2002) Photosystem II: a multisubunit membrane protein that oxidises water. Curr Opin Struct Biol 12:523–530

Bass RB, Strop P, Barclay M, Rees DC (2002) Crystal structure of *Escherichia coli* MscS, a voltage-modulated and mechanosensitive channel. Science 298:1582–1587 (PDB id 2OAU)

Ben-Shem A, Frolow F, Nelson N (2003) Crystal structure of plant photosystem I. Nature 426:630–635 (PDB id 1QZV)

Ben-Shem A, Fass D, Bibi E (2007) Structural basis for intramembrane proteolysis by rhomboid serine proteases. Proc Natl Acad Sci USA 104:462–466 (PDB id 2IRV)

Berry EA, Huang LS, Saechao LK, Pon NG, Valkova-Valchanova M, Daldal F (2004) X-ray structure of *Rhodobacter capsulatus* cytochrome bc1: comparison with its mitochondrial and chloroplast counterparts. Photosynth Res 81:251–275 (PDB id 1ZRT)

Bertero MG, Rothery RA, Palak M, Hou C, Lim D, Blasco F, Weiner JH, Strynadka NC (2003) Insights into the respiratory electron transfer pathway from the structure of nitrate reductase A. Nat Struct Biol 10:681–687 (PDB id 1Q16)

Biesiadka J, Loll B, Kern J, Irrgang K-D, Zouni A (2004) Crystal structure of cyanobacterial photosystem II at 3.2 Å resolution: a closer look at the Mn-cluster. Phys Chem Chem Phys 6:4733–4736 (PDB id 1W5C)

Billich A, Nussbaumer P, Lehr P (2000) Stimulation of MCF-7 breast cancer cell proliferation by estrone sulfate and dehydroepiandrosterone sulfate: inhibition by novel non-steroidal steroid sulfatase inhibitors. J Steroid Biochem Mol Biol 73:225–235

Blakely RD (2001) Physiological genomics of antidepressant targets: keeping the periphery in mind. J Neurosci 21:8319–8323

Blobel G (1980) Intracellular protein topogenesis. Proc Natl Acad Sci USA 77:1496–1500

Bond CS, Clements PR, Ashby SJ, Collyer CA, Harrop SJ, Hopwood JJ, Guss JM (1997) Structure of a human lysosomal sulfatase. Structure 5:277–289

Borths EL, Locher KP, Lee AT, Rees DC (2002) The structure of *Escherichia coli* BtuF and binding to its cognate ATP binding cassette transporter. Proc Natl Acad Sci USA 99:16642–16647

Boudker O, Ryan RM, Yernool D, Shimamoto K, Gouaux E (2007) Coupling substrate and ion binding to extracellular gate of a sodium-dependent aspartate transporter. Nature 445:387–393 (PDB id 2NWX)

Brown MH, Paulsen IT, Skurray RA (1999) The multidrug efflux protein NorM is a prototype of a new family of transporters. Mol Microbiol 31:394–395

Brown MS, Ye J, Rawson RB, Goldstein JL (2000) Regulated intramembrane proteolysis: a control mechanism conserved from bacteria to humans. Cell 100:391–398

Cadieux N, Bradbeer C, Reeger-Schneider E, Koster W, Mohanty AK, Wiener MC, Kadner RJ (2002) Identification of the periplasmic cobalamin-binding protein BtuF of *Escherichia coli*. J Bacteriol 184:706–717

Chandy G, Zampighi GA, Kreman M, Hall JE (1997) Comparison of the water transporting properties of MIP and AQP1. J Membr Biol 159:29–39

Chang G, Spencer RH, Lee AT, Barclay MT, Rees DC (1998) Structure of the MscL homolog from *Mycobacterium tuberculosis*: a gated mechanosensitive ion channel. Science 282:2220–2226 (PDB id 2OAR)

Chen TY, Miller C (1996) Nonequilibrium gating and voltage dependence of the ClC-0 Cl-channel. J Gen Physiol 108:237–250

Chen NH, Reith ME, Quick MW (2004) Synaptic uptake and beyond: the sodium- and chloride-dependent neurotransmitter transporter family SLC6. Pflugers Arch 447:519–531

Chen YJ, Pornillos O, Lieu S, Ma C, Chen AP, Chang G (2007) X-ray structure of EmrE supports dual topology model. Proc Natl Acad Sci USA 104:18999–19004 (PDB id 3B5D)

Cherezov V, Rosenbaum DM, Hanson MA, Rasmussen SGF, Thian FS, Kobilka TS, Choi HJ, Kuhn P, Weis WI, Kobilka BK, Stevens RC (2007) High-resolution crystal structure of an engineered human beta(2)-adrenergic G protein-coupled receptor. Science 318:1258–1265 (PDB id 2RH1)

Cogdell RJ, Isaacs NW, Freer AA, Arrelano J, Howard TD, Papiz MZ, Hawthornthwaite-Lawless AM, Prince S (1997) The structure and function of the LH2 (B800–850) complex from the purple photosynthetic bacterium *Rhodopseudomonas acidophila* strain 10050. Prog Biophys Mol Biol 68:1–27

Collins RF, Derrick JP (2007) Wza: a new structural paradigm for outer membrane secretory proteins? Trends Microbiol 15:96–100

Cuthbertson L, Mainprize IL, Naismith JH, Whitfield C (2009) Pivotal roles of the outer membrane polysaccharide export and polysaccharide copolymerase protein families in export of extracellular polysaccharides in Gram-negative bacteria. Microbiol Mol Biol Rev 73:155–177

Danbolt NC (2001) Glutamate uptake. Prog Neurobiol 65:1–105

Dawson RJP, Locher KP (2006) Structure of a bacterial multidrug ABC transporter. Nature 443:180–185 (PDB id 2HYD)

de Keyzer J, van der Does C, Kloosterman TG, Driessen AJ (2003) Direct demonstration of ATP-dependent release of SecA from a translocating preprotein by surface plasmon resonance. J Biol Chem 278:29581–29586

Deisenhofer J, Epp O, Miki K, Huber R, Michel H (1985) Structure of the protein subunits in the photosynthetic reaction centre of *Rhodopseudomonas viridis* at 3 Å resolution. Nature 318:618–624

Deisenhofer J, Epp O, Sinning I, Michel H (1995) Crystallographic refinement at 2.3 Å resolution and refined model of the photosynthetic reaction centre from *Rhodopseudomonas viridis*. J Mol Biol 246:429–457 (PDB id 1PRC)

DeLano WL (2002) The PyMOL molecular graphics system. http://www.pymol.org

Dong CJ, Beis K, Nesper J, Brunkan-LaMontagne AL, Clarke BR, Whitfield C, Naismith JH (2006) Wza the translocon for *E. coli* capsular polysaccharides defines a new class of membrane protein. Nature 444:226–229 (PDB id 2J58)

Doyle DA, Morais Cabral J, Pfuetzner RA, Kuo A, Gulbis JM, Cohen SL, Chait BT, MacKinnon R (1998) The structure of the potassium channel: molecular basis of K^+ conduction and selectivity. Science 280:69–77 (PDB id 1BL8)

Dutzler R, Campbell EB, Cadene M, Chait BT, MacKinnon R (2002) X-ray structure of a ClC chloride channel at 3.0 Å reveals the molecular basis of anion selectivity. Nature 415:287–294 (PDB id 1KPK, 1KPL)

Dutzler R, Campbell EB, MacKinnon R (2003) Gating the selectivity filter in ClC chloride channels. Science 300:108–112 (PDB id 1OTS)

Enami N, Yoshimura K, Murakami M, Okumura H, Ihara K, Kouyama T (2006) Crystal structures of archaerhodopsin-1 and -2: common structural motif in archaeal light-driven proton pumps. J Mol Biol 358:675–685 (PDB id 1VGO)

Eshaghi S, Niegowski D, Kohl A, Molina DM, Lesley SA, Nordlund P (2006) Crystal structure of a divalent metal ion transporter CorA at 2.9 Å resolution. Science 313:354–357 (PDB id 2IUB)

Esser L, Gong X, Yang SQ, Yu L, Yu CA, Xia D (2006) Surface-modulated motion switch: capture and release of iron-sulfur protein in the cytochrome bc(1) complex. Proc Natl Acad Sci USA 103:13045–13050 (PDB id 2FYN, 2FYU)

Feher G, Allen JP, Okamura MY, Rees DC (1989) Structure and function of bacterial photosynthetic reaction centers. Nature 339:111–116 (PDB id 1PSS)

Feng L, Yan HC, Wu ZR, Yan N, Wang Z, Jeffrey PD, Shi YG (2007) Structure of a site-2 protease family intramembrane metalloprotease. Science 318:1608–1612

Ferguson AD, McKeever BM, Xu S, Wisniewski D, Miller DK, Yamin TT, Spencer RH, Chu L, Ujjainwalla F, Cunningham BR, Evans JF, Becker JW (2007) Crystal structure of inhibitor-bound human 5-lipoxygenase-activating protein. Science 317:510–512 (PDB id 2Q7 M)

Ferreira KN, Iverson TM, Maghlaoui K, Barber J, Iwata S (2004) Architecture of the photosynthetic oxygen-evolving center. Science 303:1831–1838 (PDB id 1S5L)

Fritzsch G, Kampmann L, Kapaun G, Michel H (1998) Water clusters in the reaction centre of *Rhodobacter sphaeroides*. Photosynth Res 55:127–132

Fu D, Libson A, Miercke LJ, Weitzman C, Nollert P, Krucinski J, Stroud RM (2000) Structure of a glycerol-conducting channel and the basis for its selectivity. Science 290:481–486 (PDB id 1FX8)

Funk CD (2001) Prostaglandins and leukotrienes: advances in eicosanoid biology. Science 294:1871–1875

Fyfe PK, Ridge JP, McAuley KE, Cogdell RJ, Isaacs NW, Jones MR (2000) Structural consequences of the replacement of glycine M203 with aspartic acid in the reaction center from *Rhodobacter sphaeroides*. Biochemistry 39:5953–5960 (PDB id 1E14)

Fyfe PK, Isaacs NW, Cogdell RJ, Jones MR (2004) Disruption of a specific molecular interaction with a bound lipid affects the thermal stability of the purple bacterial reaction centre. Biochim Biophys Acta 1608:11–22 (PDB id 1UMX)

Gao XG, Wen XL, Esser L, Quinn B, Yu L, Yu CA, Xia D (2003) Structural basis for the quinone reduction in the bc(1) complex: a comparative analysis of crystal structures of mitochondrial

cytochrome bc(1) with bound substrate and inhibitors at the Qi site. Biochemistry 42:9067–9080 (PDB id 1NTK, 1NTM, 1NTZ, 1NU1)

Gordeliy VI, Labahn J, Moukhametzianov R, Efremov R, Granzin J, Schlesinger R, Büldt G, Savopol T, Scheidig AJ, Klare JP, Engelhard M (2002) Molecular basis of transmembrane signalling by sensory rhodopsin II-transducer complex. Nature 419:484–487 (PDB id 1H2S)

Gouaux E (2009) Review. The molecular logic of sodium-coupled neurotransmitter transporters. Philos Trans R Soc Lond B Biol Sci 364:149–154

Gropp T, Brustovetsky N, Klingenberg M, Muller V, Fendler K, Bamberg E (1999) Kinetics of electrogenic transport by the ADP/ATP carrier. Biophys J 77:714–726

Guan L, Mirza O, Verner G, Iwata S, Kaback HR (2007) Structural determination of wild-type lactose permease. Proc Natl Acad Sci USA 104:15294–15298

Guddat LW, Bardwell JC, Martin JL (1998) Crystal structures of reduced and oxidized DsbA: investigation of domain motion and thiolate stabilization. Structure 6:757–767

Hahn MK, Blakely RD (2002) Monoamine transporter gene structure and polymorphisms in relation to psychiatric and other complex disorders. Pharmacogenomics J 2:217–235

Harries WE, Akhavan D, Miercke LJ, Khademi S, Stroud RM (2004) The channel architecture of aquaporin 0 at a 2.2 Å resolution. Proc Natl Acad Sci USA 101:14045–14050 (PDB id 1YMG)

Hartigan N, Tharia HA, Sweeney F, Lawless AM, Papiz M (2002) The 7.5 Å electron density and spectroscopic properties of a novel low-light B800 LH2 from *Rhodopseudomonas palustris*. Biophys J 82:963–977

Hattori M, Tanaka Y, Fukai S, Ishitani R, Nureki O (2007) Crystal structure of the MgtE Mg^{2+} transporter. Nature 448:1072–1075 (PDB id 2YVX)

Hebert H, Jegerschold C (2007) The structure of membrane associated proteins in eicosanoid and glutathione metabolism as determined by electron crystallography. Curr Opin Struct Biol 17:396–404

Hernandez-Guzman FG, Higashiyama T, Pangborn W, Osawa Y, Ghosh D (2003) Structure of human estrone sulfatase suggests functional roles of membrane association. J Biol Chem 278:22989–22997 (PDB id 1P49)

Hoff WD, Jung KH, Spudich JL (1997) Molecular mechanism of photosignaling by archaeal sensory rhodopsins. Annu Rev Biophys Biomol Struct 26:223–258

Holland IB, Blight MA (1999) ABC-ATPases, adaptable energy generators fuelling transmembrane movement of a variety of molecules in organisms from bacteria to humans. J Mol Biol 293:381–399

Hollenstein K, Frei DC, Locher KP (2007) Structure of an ABC transporter in complex with its binding protein. Nature 446:213–216 (PDB id 2ONK)

Holm PJ, Bhakat P, Jegerschold C, Gyobu N, Mitsuoka K, Fujiyoshi Y, Morgenstern R, Hebert H (2006) Structural basis for detoxification and oxidative stress protection in membranes. J Mol Biol 360:934–945

Huang Y, Lemieux MJ, Song J, Auer M, Wang DN (2003) Structure and mechanism of the glycerol-3-phosphate transporter from *Escherichia coli*. Science 301:616–620 (PDB id 1PW4)

Huang LS, Shen JT, Wang AC, Berry EA (2006a) Crystallographic studies of the binding of ligands to the dicarboxylate site of Complex II, and the identity of the ligand in the 'oxaloacetate-inhibited' state. Biochim Et Biophys Acta-Bioenerg 1757:1073–1083 (PDB id 2H88, 2H89)

Huang LS, Sun G, Cobessi D, Wang AC, Shen JT, Tung EY, Anderson VE, Berry EA (2006b) 3-Nitropropionic acid is a suicide inhibitor of mitochondrial respiration that, upon oxidation by Complex II, forms a covalent adduct with a catalytic base arginine in the active site of the enzyme. J Biol Chem 281:5965–5972 (PDB id 1YQ3, 1YQ4, 2FBW)

Hung LW, Wang IXY, Nikaido K, Liu PQ, Ames GFL, Kim SH (1998) Crystal structure of the ATP-binding subunit of an ABC transporter. Nature 396:703–707

Hunte C, Koepke J, Lange C, Rossmanith T, Michel H (2000) Structure at 2.3 Å resolution of cytochrome bc1 complex from the yeast Saccharomyces cerevisiae co-crystallized with an antibody Fv fragment. Structure 8:669–684 (PDB id 1EZV)

Hunte C, Screpanti E, Venturi M, Rimon A, Padan E, Michel H (2005) Structure of a Na^+/H^+ antiporter and insights into mechanism of action and regulation by pH. Nature 435:1197–1202

Hvorup RN, Goetz BA, Niederer M, Hollenstein K, Perozo E, Locher KP (2007) Asymmetry in the structure of the ABC transporter-binding protein complex BtuCD–BtuF. Science 317:1387–1390 (PDB id 2QI9)

Inaba K, Murakami S, Suzuki M, Nakagawa A, Yamashita E, Okada K, Ito K (2006) Crystal structure of the DsbB–DsbA complex reveals a mechanism of disulfide bond generation. Cell 127:789–801 (PDB id 2HI7)

Iverson TM, Luna-Chavez C, Cecchini G, Rees DC (1999) Structure of the *Escherichia coli* fumerate reductase respiratory complex. Science 284:1961–1966 (PDB id 1LOV)

Iwata S, Ostermeier C, Ludwig B, Michel H (1995) Structure at 2.8-angstrom resolution of cytochrome-*c*-oxidase from *Paracoccus Denitrificans*. Nature 376:660–669 (PDB id 1AR1, 1QLE)

Iwata S, Lee JW, Okada K, Lee JK, Iwata M, Rasmussen B, Link TA, Ramaswamy S, Jap BK (1998) Complete structure of the 11-subunit bovine mitochondrial cytochrome bc_1 complex. Science 281:64–71 (PDB id 1BE3, 1BGY)

Jardetzky O (1966) Simple allosteric model for membrane pumps. Nature 211:969–970

Jasti J, Furukawa H, Gonzales EB, Gouaux E (2007) Structure of acid-sensing ion channel 1 at 1.9 Å resolution and low pH. Nature 449:316–323 (PDB id 2QTS)

Jiang Y, Pico A, Cadene M, Chait BT, MacKinnon R (2001) Structure of the RCK domain from the *E. coli* K^+ channel and demonstration of its presence in the human BK channel. Neuron 29:593–601 (PDB id 1ID1)

Jiang Y, Lee A, Chen J, Cadene M, Chait BT, MacKinnon R (2002a) Crystal structure and mechanism of a calcium-gated potassium channel. Nature 417:515–522 (PDB id 1LNQ)

Jiang Y, Lee A, Chen J, Cadene M, Chait BT, MacKinnon R (2002b) The open pore conformation of potassium channels. Nature 417:523–526

Jiang YX, Lee A, Chen JY, Ruta V, Cadene M, Chait BT, MacKinnon R (2003) X-ray structure of a voltage-dependent K^+ channel. Nature 423:33–41 (PDB id 1ORQ)

Jiang QX, Wang DN, MacKinnon R (2004) Electron microscopic analysis of KvAP voltage-dependent K^+ channels in an open conformation. Nature 430:806–810

Johansson I, Larsson C, Ek B, Kjellbom P (1996) The major integral proteins of spinach leaf plasma membranes are putative aquaporins and are phosphorylated in response to Ca^{2+} and apoplastic water potential. Plant Cell 8:1181–1191

Johansson I, Karlsson M, Shukla VK, Chrispeels MJ, Larsson C, Kjellbom P (1998) Water transport activity of the plasma membrane aquaporin PM28A is regulated by phosphorylation. Plant Cell 10:451–459

Jordan P, Fromme P, Witt HT, Klukas O, Saenger W, Krauss N (2001) Three-dimensional structure of cyanobacterial photosystem I at 2.5 Å resolution. Nature 411:909–917 (PDB id 1JB0)

Jormakka M, Tornroth S, Byrne B, Iwata S (2002) Molecular basis of proton motive force generation: structure of formate dehydrogenase-N. Science 295:1863–1868 (PDB id 1KQF, 1KQG)

Kamiya N, Shen JR (2003) Crystal structure of oxygen-evolving photosystem II from *Thermosynechococcus vulcanus* at 3.7-Å resolution. Proc Natl Acad Sci USA 100:98–103 (PDB id 1IZL)

Kanai Y, Hediger MA (2004) The glutamate/neutral amino acid transporter family SLC1: molecular, physiological and pharmacological aspects. Pflugers Arch 447:469–479

Khademi S, O'Connell J 3rd, Remis J, Robles-Colmenares Y, Miercke LJ, Stroud RM (2004) Mechanism of ammonia transport by Amt/MEP/Rh: structure of AmtB at 1.35 Å. Science 305:1587–1594 (PDB id 1U7G)

King LS, Kozono D, Agre P (2004) From structure to disease: the evolving tale of aquaporin biology. Nat Rev Mol Cell Biol 5:687–698

Kobayashi T, Kishigami S, Sone M, Inokuchi H, Mogi T, Ito K (1997) Respiratory chain is required to maintain oxidized states of the DsbA–DsbB disulfide bond formation system in aerobically growing *Escherichia coli* cells. Proc Natl Acad Sci USA 94:11857–11862

Koepke J, Hu XC, Muenke C, Schulten K, Michel H (1996) The crystal structure of the light-harvesting complex II (B800–850) from *Rhodospirillum molischianum*. Structure 4:581–597 (PDB id 1LGH)

Kolbe M, Besir H, Essen L-O, Oesterhelt D (2000) Structure of the light-driven chloride pump halorhodopsin at 1.8 Å. Science 288:1390–1396 (PDB id 1E12)

Kuhlbrandt W (2004) Biology, structure and mechanism of P-type ATPases. Nat Rev Mol Cell Biol 5:282–295

Kuo AL, Gulbis JM, Antcliff JF, Rahman T, Lowe ED, Zimmer J, Cuthbertson J, Ashcroft FM, Ezaki T, Doyle DA (2003) Crystal structure of the potassium channel KirBac1.1 in the closed state. Science 300:1922–1926 (PDB id 1P7B)

Kurisu G, Zhang H, Smith JL, Cramer WA (2003) Structure of the cytochrome b6f complex of oxygenic photosynthesis: tuning the cavity. Science 302:1009–1014 (PDB id 1VF5)

Lancaster CRD, Bibikova MV, Sabatino P, Oesterhelt D, Michel H (2000) Structural basis of the drastically increased initial electron transfer rate in the reaction center from a *Rhodopseudomonas viridis* mutant described at 2.00-Å resolution. J Biol Chem 275:39364–39368 (PDB id 1DXR)

Lange C, Hunte C (2002) Crystal structure of the yeast cytochrome bc(1) complex with its bound substrate cytochrome *c*. Proc Natl Acad Sci USA 99:2800–2805 (PDB id 1KYO)

Lemieux MJ, Fischer SJ, Cherney MM, Bateman KS, James MNG (2007) The crystal structure of the rhomboid peptidase from *Haemophilus influenzae* provides insight into intramembrane proteolysis. Proc Natl Acad Sci USA 104:750–754 (PDB id 2NR9)

Li J, Edwards PC, Burghammer M, Villa C, Schertler GF (2004) Structure of bovine rhodopsin in a trigonal crystal form. J Mol Biol 343:1409–1438 (PDB id 1GZM)

Li L, Mustafi D, Fu Q, Tereshko V, Chen DL, Tice JD, Ismagilov RF (2006) Nanoliter microfluidic hybrid method for simultaneous screening and optimization validated with crystallization of membrane proteins. Proc Natl Acad Sci USA 103:19243–19248

Li X, Jayachandran S, Nguyen HH, Chan MK (2007) Structure of the *Nitrosomonas europaea* Rh protein. Proc Natl Acad Sci USA 104:19279–19284

Lieberman RL, Rosenzweig AC (2005) Crystal structure of a membrane-bound metalloenzyme that catalyses the biological oxidation of methane. Nature 434:177–182 (PDB id 1YEW)

Liu Z, Yan H, Wang K, Kuang T, Zhang J, Gui L, An X, Chang W (2004) Crystal structure of spinach major light-harvesting complex at 2.72 Å resolution. Nature 428:287–292 (PDB id 1RWT)

Locher KP, Borths E (2004) ABC transporter architecture and mechanism: implications from the crystal structures of BtuCD and BtuF. FEBS Lett 564:264–268

Locher KP, Lee AT, Rees DC (2002) The *E. coli* BtuCD structure: a framework for ABC transporter architecture and mechanism. Science 296:1091–1098 (PDB id 1L7 V)

Lomize MA, Lomize AL, Pogozheva ID, Mosberg HI (2006) OPM: Orientations of proteins in membranes database. Bioinformatics 22:623–625

Long SB, Campbell EB, MacKinnon R (2005a) Crystal structure of a mammalian voltage-dependent Shaker family K^+ channel. Science 309:897–903 (PDB id 2A79)

Long SB, Campbell EB, MacKinnon R (2005b) Voltage sensor of Kv1.2: structural basis of electromechanical coupling. Science 309:903–908

Long SB, Tao X, Campbell EB, MacKinnon R (2007) Atomic structure of a voltage-dependent K^+ channel in a lipid membrane-like environment. Nature 450:376–382 (PDB id 2R9R)

Lu M, Fu D (2007) Structure of the zinc transporter YiiP. Science 317:1746–1748 (PDB id 2QFI)

Luecke H, Schobert B, Richter HT, Cartailler P, Lanyi JK (1999) Structure of bacteriorhodopsin at 1.55 Å resolution. J Mol Biol 291:899–911 (PDB id 1C3 W)

Luecke H, Schobert B, Lanyi JK, Spudich EN, Spudich JL (2001) Crystal structure of sensory rhodopsin II at 2.4 Å: insights into color tuning and transducer interaction. Science 293:1499–1503 (PDB id 1JGJ)

Lukatela G, Krauss N, Theis K, Selmer T, Gieselmann V, von Figura K, Saenger W (1998) Crystal structure of human arylsulfatase A: the aldehyde function and the metal ion at the active site suggest a novel mechanism for sulfate ester hydrolysis. Biochemistry 37:3654–3664

Lunin VV, Dobrovetsky E, Khutoreskaya G, Zhang R, Joachimiak A, Doyle DA, Bochkarev A, Maguire ME, Edwards AM, Koth CM (2006) Crystal structure of the CorA Mg2+ transporter. Nature 440:833–837 (PDB id 2BBH)

Lupo D, Li XD, Durand A, Tomizaki T, Cherif-Zahar B, Matassi G, Merrick M, Winkler FK (2007) The 1.3 Å resolution structure of *Nitrosomonas europaea* Rh50 and mechanistic implications for NH3 transport by Rhesus family proteins. Proc Natl Acad Sci USA 104:19303–19308

Ma T, Yang B, Verkman AS (1997) Cloning of a novel water and urea-permeable aquaporin from mouse expressed strongly in colon, placenta, liver, and heart. Biochem Biophys Res Commun 240:324–328

Madej MG, Nasiri HR, Hilgendorff NS, Schwalbe H, Lancaster CRD (2006) Evidence for transmembrane proton transfer in a dihaem-containing membrane protein complex. EMBO J 25:4963–4970 (PDB id 2BS2)

Martinez Molina D, Wetterholm A, Kohl A, McCarthy AA, Niegowski D, Ohlson E, Hammarberg T, Eshaghi S, Haeggstrom JZ, Nordlund P (2007) Structural basis for synthesis of inflammatory mediators by human leukotriene C4 synthase. Nature 448:613–616 (PDB id 2UUH)

Maser P, Thomine S, Schroeder JI, Ward JM, Hirschi K, Sze H, Talke IN, Amtmann A, Maathuis FJ, Sanders D, Harper JF, Tchieu J, Gribskov M, Persans MW, Salt DE, Kim SA, Guerinot ML (2001) Phylogenetic relationships within cation transporter families of *Arabidopsis*. Plant Physiol 126:1646–1667

McAuley KE, Fyfe PK, Ridge JP, Cogdell RJ, Isaacs NW, Jones MR (2000) Ubiquinone binding, ubiquinone exclusion, and detailed cofactor conformation in a mutant bacterial reaction center. Biochemistry 39:15032–15043 (PDB id 1QOV)

McAuley-Hecht KE, Fyfe PK, Ridge JP, Prince SM, Hunter CN, Isaacs NW, Cogdell RJ, Jones MR (1998) Structural studies of wild-type and mutant reaction centers from an antenna-deficient strain of *Rhodobacter sphaeroides*: monitoring the optical

properties of the complex from bacterial cell to crystal. Biochemistry 37:4740–4750 (PDB id 1MPS)
McDermott G, Prince SM, Freer AA, Hawthornthwaite-Lawless AM, Papiz MZ, Cogdell RJ, Isaacs NW (1995) Crystal structure of an integral membrane light-harvesting complex from photosynthetic bacteria. Nature 374:517–521 (PDB id 1KZU)
McLuskey K, Prince SM, Cogdell RJ, Isaacs NW (2001) The crystallographic structure of the B800–820 LH3 light-harvesting complex from the purple bacteria *Rhodopseudomonas Acidophila* strain 7050. Biochemistry 40:8783–8789 (PDB id 1IJD)
Meier T, Polzer P, Diederichs K, Welte W, Dimroth P (2005) Structure of the rotor ring of F-Type Na^+-ATPase from *Ilyobacter tartaricus*. Science 308:659–662 (PDB id 1YCE)
Meinild AK, Klaerke DA, Zeuthen T (1998) Bidirectional water fluxes and specificity for small hydrophilic molecules in aquaporins 0–5. J Biol Chem 273:32446–32451
Merkx M, Kopp DA, Sazinsky MH, Blazyk JL, Muller J, Lippard SJ (2001) Dioxygen activation and methane hydroxylation by soluble methane monooxygenase: a tale of two irons and three proteins A list of abbreviations can be found in Section 7. Angew Chem Int Ed Engl 40:2782–2807
Michel H (1982) Three-dimensional crystals of a membrane protein complex; the photosynthetic reaction center from *Rhodopseudomonas viridis*. J Mol Biol 158:567–572
Moncoq K, Trieber CA, Young HS (2007) The molecular basis for cyclopiazonic acid inhibition of the sarcoplasmic reticulum calcium pump. J Biol Chem 282:9748–9757 (PDB id 2O9 J, 2OA0)
Morth JP, Pedersen BP, Toustrup-Jensen MS, Sorensen TLM, Petersen J, Andersen JP, Vilsen B, Nissen P (2007) Crystal structure of the sodium–potassium pump. Nature 450:1043–1049 (PDB id 3B8E)
Murakami S, Nakashima R, Yamashita E, Yamaguchi A (2002) Crystal structure of bacterial multidrug efflux transporter AcrB. Nature 419:587–593
Murakami S, Nakashima R, Yamashita E, Matsumoto T, Yamaguchi A (2006) Crystal structures of a multidrug transporter reveal a functionally rotating mechanism. Nature 443:173–179 (PDB id 2DHH)
Murata T, Yamato I, Kakinuma Y, Leslie AG, Walker JE (2005) Structure of the rotor of the V-Type Na^+-ATPase from *Enterococcus hirae*. Science 308:654–659 (PDB id 2BL2)
Nemeth-Cahalan KL, Hall JE (2000) pH and calcium regulate the water permeability of aquaporin 0. J Biol Chem 275:6777–6782
Nikaido H (1996) Multidrug efflux pumps of Gram-negative bacteria. J Bacteriol 178:5853–5859
Nikaido H (1998) Multiple antibiotic resistance and efflux. Curr Opin Microbiol 1:516–523
Nishida M, Cadene M, Chait BT, MacKinnon R (2007) Crystal structure of a Kir3.1-prokaryotic Kir channel chimera. EMBO J 26:4005–4015 (PDB id 1XL4)
Nogi T, Fathir I, Kobayashi M, Nozawa T, Miki K (2000) Crystal structures of photosynthetic reaction center and high-potential iron-sulfur protein from *Thermochromatium tepidum*: thermostability and electron transfer. Proc Natl Acad Sci USA 97:13561–13566 (PDB id 1EYS)
Nury H, Dahout-Gonzalez C, Trezeguet V, Lauquin G, Brandolin G, Pebay-Peyroula E (2005) Structural basis for lipid-mediated interactions between mitochondrial ADP/ATP carrier monomers. FEBS Lett 579:6031–6036
Okada T, Fujiyoshi Y, Silow M, Navarro J, Landau EM, Shichida Y (2002) Functional role of internal water molecules in rhodopsin revealed by X-ray crystallography. Proc Natl Acad Sci USA 99:5982–5987
Okada T, Sugihara M, Bondar AN, Elstner M, Entel P, Buss V (2004) The retinal conformation and its environment in rhodopsin in light of a new 2.2 Å crystal structure. J Mol Biol 342:571–583 (PDB id 1U19)
Oldham ML, Khare D, Quiocho FA, Davidson AL, Chen J (2007) Crystal structure of a catalytic intermediate of the maltose transporter. Nature 450:515–521 (PDB id 2R6G)
Olesen C, Picard M, Winther AML, Gyrup C, Morth JP, Oxvig C, Moller JV, Nissen P (2007) The structural basis of calcium transport by the calcium pump. Nature 450:1036–1042 (PDB id 3B9B, 3BA6, 3B9R)
Ou X, Blount P, Hoffman RJ, Kung C (1998) One face of a transmembrane helix is crucial in mechanosensitive channel gating. Proc Natl Acad Sci USA 95:11471–11475
Padan E, Tzubery T, Herz K, Kozachkov L, Rimon A, Galili L (2004) NhaA of *Escherichia coli*, as a model of a pH-regulated Na^+/H^+ antiporter. Biochim Biophys Acta 1658:2–13
Palczewski K, Kumasaka T, Hori T, Behnke CA, Motoshima H, Fox BA, Le Trong I, Teller DC, Okada T, Stenkamp RE, Yamamoto M, Miyano M (2000) Crystal structure of rhodopsin: a G protein-coupled receptor. Science 289:739–745 (PDB id 1F88)
Palsdottir H, Lojero CG, Trumpower BL, Hunte C (2003) Structure of the yeast cytochrome bc(1) complex with a hydroxyquinone anion Q(o) site inhibitor bound. J Biol Chem 278:31303–31311 (PDB id 1P84)
Papiz MZ, Prince SM, Howard TD, Cogdell RJ, Isaacs NW (2003) The structure and thermal motion of the B800–850 LH2 complex from Rps. acidophila at 2.0 Å resolution and 100 K: new structural features and functionally relevant motions. J Mol Biol 326:1523–1538 (PDB id 1NKZ)
Parenti G, Meroni G, Ballabio A (1997) The sulfatase gene family. Curr Opin Genet Dev 7:386–391
Pearson WR (2005) Phylogenies of glutathione transferase families. Methods Enzymol 401:186–204
Pebay-Peyroula E, Rummel G, Rosenbusch JP, Landau EM (1997) X-ray structure of bacteriorhodopsin at 2.5 Å from microcrystals grown in lipidic cubic phases. Science 277:1676–1681 (PDB id 1APQ)
Pebay-Peyroula E, Dahout-Gonzalez C, Kahn R, Trezeguet V, Lauquin GJ, Brandolin G (2003) Structure of mitochondrial ADP/ATP carrier in complex with carboxyatractyloside. Nature 426:39–44
Pedersen BP, Buch-Pedersen MJ, Morth JP, Palmgren MG, Nissen P (2007) Crystal structure of the plasma membrane proton pump. Nature 450:1111–1114 (PDB id 3B8C)
Peng J, Huang CH (2006) Rh proteins vs Amt proteins: an organismal and phylogenetic perspective on CO2 and NH3 gas channels. Transfus Clin Biol 13:85–94
Pinkett HW, Lee AT, Lum P, Locher KP, Rees DC (2007) An inward-facing conformation of a putative metal-chelate-type ABC transporter. Science 315:373–377 (PDB id 2NQ2)
Prince SM, Papiz MZ, Freer AA, McDermott G, Hawthornthwaite-Lawless AM, Cogdell RJ, Isaacs NW (1997) Apoprotein structure in the LH2 complex from *Rhodopseudomonas acidophila* strain 10050: modular assembly and protein pigment interactions. J Mol Biol 268:412–423 (PDB id 1KZU)
Pusch M, Ludewig U, Rehfeldt A, Jentsch TJ (1995) Gating of the voltage-dependent chloride channel CIC-0 by the permeant anion. Nature 373:527–531
Pusch M, Zifarelli G, Murgia AR, Picollo A, Babini E (2006) Channel or transporter? The CLC saga continues. Exp Physiol 91:149–152
Putman M, van Veen HW, Konings WN (2000) Molecular properties of bacterial multidrug transporters. Microbiol Mol Biol Rev 64:672–693
Qin L, Hiser C, Mulichak A, Garavito RM, Ferguson-Miller S (2006) Identification of conserved lipid/detergent-binding sites in a high-resolution structure of the membrane protein cytochrome *c*

oxidase. Proc Natl Acad Sci USA 103:16117–16122 (PDB id 2GSM)

Rapoport TA, Jungnickel B, Kutay U (1996) Protein transport across the eukaryotic endoplasmic reticulum and bacterial inner membranes. Annu Rev Biochem 65:271–303

Rapp M, Seppala S, Granseth E, von Heijne G (2007) Emulating membrane protein evolution by rational design. Science 315:1282–1284

Rasmussen SGF, Choi HJ, Rosenbaum DM, Kobilka TS, Thian FS, Edwards PC, Burghammer M, Ratnala VRP, Sanishvili R, Fischetti RF, Schertler GFX, Weis WI, Kobilka BK (2007) Crystal structure of the human beta(2) adrenergic G-protein-coupled receptor. Nature 450:383–387 (PDB id 2R4R, 2R4S)

Richerson GB, Wu Y (2004) Role of the GABA transporter in epilepsy. Adv Exp Med Biol 548:76–91

Ridge JP, Fyfe PK, McAuley KE, van Brederode ME, Robert B, van Grondelle R, Isaacs NW, Cogdell RJ, Jones MR (2000) An examination of how structural changes can affect the rate of electron transfer in a mutated bacterial photoreaction centre. Biochem J 351:567–578 (PDB id 1E6D)

Ripoche P, Bertrand O, Gane P, Birkenmeier C, Colin Y, Cartron JP (2004) Human Rhesus-associated glycoprotein mediates facilitated transport of NH(3) into red blood cells. Proc Natl Acad Sci USA 101:17222–17227

Roszak AW, Howard TD, Southall J, Gardiner AT, Law CJ, Isaacs NW, Cogdell RJ (2003) Crystal structure of the RC-LH1 core complex from *Rhodopseudomonas palustris*. Science 302:1969–1972 (PDB id 1PYH)

Roszak AW, McKendrick K, Gardiner AT, Mitchell IA, Isaacs NW, Cogdell RJ, Hashimoto H, Frank HA (2004) Protein regulation of carotenoid binding: gatekeeper and locking amino acid residues in reaction centers of *Rhodobacter sphaeroides*. Structure 12:765–773 (PDB id 1RG5, 1RGN, 1RQK)

Royant A, Nollert P, Edman K, Neutze R, Landau EM, Pebay-Peyroula E (2001) X-ray structure of sensory rhodopsin II at 2.1-Å resolution. Proc Natl Acad Sci USA 98:10131–10136 (PDB id 1H68)

Saier MH Jr (2000) Families of proteins forming transmembrane channels. J Membr Biol 175:165–180

Salom D, Lodowski DT, Stenkamp RE, Le Trong I, Golczak M, Jastrzebska B, Harris T, Ballesteros JA, Palczewski K (2006) Crystal structure of a photoactivated deprotonated intermediate of rhodopsin. Proc Natl Acad Sci USA 103:16123–16128

Samuelsson B (1983) Leukotrienes: mediators of immediate hypersensitivity reactions and inflammation. Science 220:568–575

Samuelsson B, Dahlen SE, Lindgren JA, Rouzer CA, Serhan CN (1987) Leukotrienes and lipoxins: structures, biosynthesis, and biological effects. Science 237:1171–1176

Savage DF, Egea PF, Robles-Colmenares Y, O'Connell JD 3rd, Stroud RM (2003) Architecture and selectivity in aquaporins: 2.5 Å X-ray structure of aquaporin Z. PLoS Biol 1:334–340 (PDB id 1RC2)

Schuldiner S, Granot D, Mordoch SS, Ninio S, Rotem D, Soskin M, Tate CG, Yerushalmi H (2001) Small is mighty: EmrE, a multidrug transporter as an experimental paradigm. News Physiol Sci 16:130–134

Seeger MA, Schiefner A, Eicher T, Verrey F, Diederichs K, Pos KM (2006) Structural asymmetry of AcrB trimer suggests a peristaltic pump mechanism. Science 313:1295–1298 (PDB id 2GIF)

Shi N, Ye S, Alam A, Chen L, Jiang Y (2006) Atomic structure of a Na^{+-} and K^{+-} conducting channel. Nature 440:570–574 (PDB id 2AHY)

Sigworth FJ (1994) Voltage gating of ion channels. Q Rev Biophys 27:1–40

Singh SK, Yamashita A, Gouaux E (2007) Antidepressant binding site in a bacterial homologue of neurotransmitter transporters. Nature 448:952–956 (PDB id 2Q6H)

Slepkov ER, Rainey JK, Sykes BD, Fliegel L (2007) Structural and functional analysis of the Na+/H+ exchanger. Biochem J 401:623–633

Slotboom DJ, Konings WN, Lolkema JS (1999) Structural features of the glutamate transporter family. Microbiol Mol Biol Rev 63:293–307

Smith JL, Zhang H, Yan J, Kurisu G, Cramer WA (2004) Cytochrome bc complexes: a common core of structure and function surrounded by diversity in the outlying provinces. Curr Opin Struct Biol 14:432–439

Sørensen TL, Møller JV, Nissen P (2004) Phosphoryl transfer and calcium ion occlusion in the calcium pump. Science 304:1672–1675 (PDB id 1T5S, 1T5T)

Soulimane T, Buse G, Bourenkov GP, Bartunik HD, Huber R, Than ME (2000) Structure and mechanism of the aberrant ba(3)-cytochrome *c* oxidase from *Thermus thermophilus*. EMBO J 19:1766–1776 (PDB id 1EHK)

Soupene E, Lee H, Kustu S (2002) Ammonium/methylammonium transport (Amt) proteins facilitate diffusion of NH3 bidirectionally. Proc Natl Acad Sci USA 99:3926–3931

Soupene E, Inwood W, Kustu S (2004) Lack of the Rhesus protein Rh1 impairs growth of the green alga *Chlamydomonas reinhardtii* at high CO2. Proc Natl Acad Sci USA 101:7787–7792

Speer BS, Shoemaker NB, Salyers AA (1992) Bacterial-resistance to tetracycline—mechanisms, transfer, and clinical-significance. Clin Microbiol Rev 5:387–399

Spiedel D, Roszak AW, McKendrick K, McAuley KE, Fyfe PK, Nabedryk E, Breton J, Robert B, Cogdell RJ, Isaacs NW, Jones MR (2002) Tuning of the optical and electrochemical properties of the primary donor bacteriochlorophylls in the reaction centre from *Rhodobacter sphaeroides*: spectroscopy and structure. Biochim Biophys Acta 1554:75–93

Spudich JL, Yang CS, Jung KH, Spudich EN (2000) Retinylidene proteins: structures and functions from archaea to humans. Annu Rev Cell Dev Biol 16:365–392

Stock D, Leslie AG, Walker JE (1999) Molecular architecture of the rotary motor in ATP synthase. Science 286:1700–1705 (PDB id 1QO1)

Stowell MHB, McPhillips TM, Rees DC, Soltis SM, Abresch EC, Feher G (1997) Light-induced structural changes in photosynthetic reaction center: implications for mechanism of electron-proton transfer. Science 276:812–816 (PDB id 1AIG, 1AIJ)

Stroebel D, Choquet Y, Popot JL, Picot D (2003) An atypical haem in the cytochrome b(6)f complex. Nature 426:413–418 (PDB id 1Q90)

Sui H, Han BG, Lee JK, Walian P, Jap BK (2001) Structural basis of water-specific transport through the AQP1 water channel. Nature 414:872–878 (PDB id 1J4 N)

Sukharev S, Betanzos M, Chiang CS, Guy HR (2001) The gating mechanism of the large mechanosensitive channel MscL. Nature 409:720–724

Sun F, Huo X, Zhai Y, Wang A, Xu J, Su D, Bartlam M, Rao Z (2005) Crystal structure of mitochondrial respiratory membrane protein complex II. Cell 121:1043–1057 (PDB id 1ZOY, 1ZPO)

Tornroth-Horsefield S, Wang Y, Hedfalk K, Johanson U, Karlsson M, Tajkhorshid E, Neutze R, Kjellbom P (2006) Structural mechanism of plant aquaporin gating. Nature 439:688–694 (PDB id 1Z98)

Tornroth-Horsefield S, Gourdon P, Horsefield R, Brive L, Yamamoto N, Mori H, Snijder A, Neutze R (2007) Crystal structure of AcrB in complex with a single transmembrane subunit reveals another twist. Structure 15:1663–1673 (PDB id 2RDD)

Tournaire-Roux C, Sutka M, Javot H, Gout E, Gerbeau P, Luu DT, Bligny R, Maurel C (2003) Cytosolic pH regulates root water transport during anoxic stress through gating of aquaporins. Nature 425:393–397

Townsend DE, Esenwine AJ, George J 3rd, Bross D, Maguire ME, Smith RL (1995) Cloning of the mgtE Mg^{2+} transporter from *Providencia stuartii* and the distribution of mgtE in Gram-negative and Gram-positive bacteria. J Bacteriol 177:5350–5354

Toyoshima C, Mizutani T (2004) Crystal structure of the calcium pump with a bound ATP analogue. Nature 430:529–535

Toyoshima C, Nakasako M, Nomura H, Ogawa H (2000) Crystal structure of the calcium pump of sarcoplasmic reticulum at 2.6 Å resolution. Nature 405:647–655 (PDB id 1SU4)

Toyoshima C, Nomura H, Tsuda T (2004) Lumenal gating mechanism revealed in calcium pump crystal structures with phosphate analogues. Nature 432:361–368 (PDB id 1WPG)

Tsukihara T, Aoyama H, Yamashita E, Tomizaki T, Yamaguchi H, Shinzawa-Itoh K, Nakashima R, Yaono R, Yoshikawa S (1995) Structures of metal sites of oxidized bovine heart cytochrome *c* oxidase at 2.8 Å. Science 269:1069–1074

Tsukihara T, Aoyama H, Yamashita E, Tomizaki T, Yamaguchi H, Shinzawa-Itoh K, Nakashima R, Yaono R, Yoshikawa S (1996) The whole structure of the 13-subunit oxidized cytochrome *c* oxidase at 2.8 Å. Science 272:1136–1144 (PDB id 1OCC)

Van den Berg B, Clemons WM Jr, Collinson I, Modis Y, Hartmann E, Harrison SC, Rapoport TA (2004) X-ray structure of a protein-conducting channel. Nature 427:36–44

Vogeley L, Sineshchekov OA, Trivedi VD, Sasaki J, Spudich JL, Luecke H (2004) Anabaena sensory rhodopsin: a photochromic color sensor at 2.0 Å. Science 306:1390–1393 (PDB id 1XIO)

von Wiren N, Gazzarrini S, Gojon A, Frommer WB (2000) The molecular physiology of ammonium uptake and retrieval. Curr Opin Plant Biol 3:254–261

Waldmann R, Champigny G, Bassilana F, Heurteaux C, Lazdunski M (1997) A proton-gated cation channel involved in acid-sensing. Nature 386:173–177

Walker JE, Runswick MJ (1993) The mitochondrial transport protein superfamily. J Bioenerg Biomembr 25:435–446

Wang YC, Zhang YJ, Ha Y (2006) Crystal structure of a rhomboid family intramembrane protease. Nature 444:179–183 (PDB id 2IC8)

Ward A, Reyes CL, Yu J, Roth CB, Chang G (2007) Flexibility in the ABC transporter MsbA: alternating access with a twist. Proc Natl Acad Sci USA 104:19005–19010 (PDB id 3B60, 3B5 W, 3B5X)

White SH (2006) Rhomboid intramembrane protease structures galore!. Nat Struct Mol Biol 13:1049–1051

White S (2009) Membrane proteins of known structure. http://blanco.biomol.uci.edu/Membrane_Proteins_xtal.html

Wu ZR, Yan N, Feng L, Oberstein A, Yan HC, Baker RP, Gu LC, Jeffrey PD, Urban S, Shi YG (2006) Structural analysis of a rhomboid family intramembrane protease reveals a gating mechanism for substrate entry. Nat Struct Mol Biol 13:1084–1091 (PDB id 2NRF)

Xia D, Yu C-A, Kim H, Xia J-Z, Kachurin AM, Zhang L, Yu L, Deisenhofer J (1997) Crystal structure of the cytochrome bc1 complex from bovine heart mitochondria. Science 277:60–66 (PDB id 1QCR)

Xia XM, Fakler B, Rivard A, Wayman G, Johnson-Pais T, Keen JE, Ishii T, Hirschberg B, Bond CT, Lutsenko S, Maylie J, Adelman JP (1998) Mechanism of calcium gating in small-conductance calcium-activated potassium channels. Nature 395:503–507

Xu Q, Axelrod HL, Abresch EC, Paddock ML, Okamura MY, Feher G (2004) X-ray structure determination of three mutants of the bacterial photosynthetic reaction centers from Rb. sphaeroides: altered proton transfer pathways. Structure 12:703–715 (PDB id 1RVJ, 1RY5, 1RZH, 1RZZ, 1S00)

Yamashita A, Singh SK, Kawate T, Jin Y, Gouaux E (2005) Crystal structure of a bacterial homologue of Na(+)/Cl(−)-dependent neurotransmitter transporters. Nature 437:215–223 (PDB id 2A65)

Yamashita E, Zhang H, Cramer WA (2007) Structure of the cytochrome b(6)f complex: quinone analogue inhibitors as ligands of heme c(n). J Mol Biol 370:39–52 (PDB id 2E74, 2E75, 2E76)

Yan JS, Kurisu G, Cramer WA (2006) Intraprotein transfer of the quinone analogue inhibitor 2,5-dibromo-3-methyl-6-isopropyl-*p*-benzoquinone in the cytochrome b(6)f complex. Proc Natl Acad Sci USA 103:69–74 (PDB id 2D2C)

Yankovskaya V, Horsefield R, Tornroth S, Luna-Chavez C, Miyoshi H, Leger C, Byrne B, Cecchini G, Iwata S (2003) Architecture of succinate dehydrogenase and reactive oxygen species generation. Science 299:700–704 (PDB id 1NEK, 1NEN)

Yasui M, Hazama A, Kwon TH, Nielsen S, Guggino WB, Agre P (1999) Rapid gating and anion permeability of an intracellular aquaporin. Nature 402:184–187

Yernool D, Boudker O, Jin Y, Gouaux E (2004) Structure of a glutamate transporter homologue from *Pyrococcus horikoshii*. Nature 431:811–818

Yerushalmi H, Schuldiner S (2000) An essential glutamyl residue in EmrE, a multidrug antiporter from *Escherichia coli*. J Biol Chem 275:5264–5269

Yerushalmi H, Lebendiker M, Schuldiner S (1995) EmrE, an *Escherichia coli* 12-kDa multidrug transporter, exchanges toxic cations and H^+ and is soluble in organic solvents. J Biol Chem 270:6856–6863

Yin Y, He X, Szewczyk P, Nguyen T, Chang G (2006) Structure of the multidrug transporter EmrD from *Escherichia coli*. Science 312:741–744 (PDB id 2GFP)

Yoshikawa S, Shinzawa-Itoh K, Nakashima R, Yaono R, Yamashita E, Inoue N, Yao M, Fei MJ, Libeu CP, Mizushima T, Yamaguchi H, Tomizaki T, Tsukihara T (1998) Redox-coupled crystal structural changes in bovine heart cytochrome *c* oxidase. Science 280:1723–1729 (PDB id 2OCC, 1OCO, 1OCR, 1OCZ)

Yu EW, McDermott G, Zgurskaya HI, Nikaido H, Koshland DE Jr (2003) Structural basis of multiple drug-binding capacity of the AcrB multidrug efflux pump. Science 300:976–980

Zhang ZL, Huang LS, Shulmeister VM, Chi Y-I, Kim KK, Hung L-W, Crofts AR, Berry EA, Kim S–H (1998) Electron transfer by domain movement in cytochrome bc1. Nature 392:677–684 (PDB id 1BCC, 2BCC, 3BCC)

Zheng L, Kostrewa D, Berneche S, Winkler FK, Li XD (2004) The mechanism of ammonia transport based on the crystal structure of AmtB of *Escherichia coli*. Proc Natl Acad Sci USA 101:17090–17095 (PDB id 1XQE)

Zhou Y, Morais-Cabral JH, Kaufman A, MacKinnon R (2001) Chemistry of ion coordination and hydration revealed by a K^+ channel-Fab complex at 2.0 Å resolution. Nature 414:43–48 (PDB id 1K4C, 1K4D)

Zhou Z, Zhen J, Karpowich NK, Goetz RM, Law CJ, Reith MEA, Wang DN (2007) LeuT-desipramine structure reveals how antidepressants block neurotransmitter reuptake. Science 317:1390–1393 (PDB id 2QJU)

Zidi-Yahiaoui N, Mouro-Chanteloup I, D'Ambrosio AM, Lopez C, Gane P, Le van Kim C, Cartron JP, Colin Y, Ripoche P (2005) Human Rhesus B and Rhesus C glycoproteins: properties of facilitated ammonium transport in recombinant kidney cells. Biochem J 391:33–40